YUNIBESITI YA BOKONE-BOPHIRIMA
NORTH-WEST UNIVERSITY
NOORDWES-UNIVERSITEIT

MATERIAL SELECTION AND OPTIMISATION OF A HIGH-TEMPERURE COMPACT HEAT EXCHANGER

J. van Greuning B.Eng.

Mini dissertation submitted in partial fulfillment of the degree
Magister of Engineering
at the
School of Mechanical and Materials Engineering,
of the
North-West University.

Supervisor: Prof. J Markgraaff

Assistant Supervisor: Prof. PG Rousseau

March 2006

Potchefstroom

ABSTRACT

Title	:	Material selection and optimisation of a high-temperature compact heat exchanger.
Author	:	J. van Greuning
Supervisor	:	Prof. J. Markgraaff
Assistant Supervisor	:	Prof. P.G. Rousseau
School	:	School of Mechanical Engineering
Degree	:	Master of Engineering

The Pebble Bed Micro Model (PBMM) plant currently employs a large conventional shell-and-tube heat exchanger as recuperator at the inlet to the heat source in order to pre-heat the nitrogen. The thermal inertia of the current PBMM recuperator influences the dynamic behaviour of the plant and the heat exchanger configuration is also different from the actual Pebble Bed Modular Reactor (PBMR) plant, which will employ a compact heat exchanger.

A need therefore exists to design a high-temperature compact heat exchanger for the PBMM plant. This study includes the material selection and optimization of the proposed heat exchanger design.

The material chosen for this recuperator is a tungsten-copper alloy with 68 wt% W and 32 wt% Cu. A mini-channel heat exchanger with a counterflow configuration is the chosen type of heat exchanger. The heat exchanger is made up of two types of plates that are stacked alternatively. These plates are then either diffusion bonded or brazed in order to form the complete heat exchanger.

The final geometry of the recuperator is as follows:

- Total length = 0.75 m
- Total width = 0.518 m
- Total height = 0.8 m

- Number of channels wide = 370
- Number of hot channels high = 200
- Number of cold channels high = 200
- Plate thickness = 1 mm
- Fin thickness = 0.4 mm
- Channel height = 1 mm
- Channel width = 1 mm

The proposed recuperator only occupies 10% of the footprint area and 13% of the volume of the shell-and-tube recuperator. Its effectivity is 95%, which results in an increase of 2% in the cycle effectivity. The response time for the compact recuperator is about 25% that of the shell-and-tube recuperator.

OPSOMMING

Titel	:	"Material selection and optimization of a high-temperature compact heat exchanger."
Outeur	:	J. van Greuning
Studieleier	:	Prof. J. Markgraaff
Hulp-studieleier	:	Prof. P.G. Rousseau
Skool	:	Meganiese Ingenieurswese
Graad	:	Magister in Ingenieurswese

Huidiglik is daar 'n konvensionele huls-en-buis hitteruiler as rekuperator in die PBMM siklus. Die rekuperator is net voor die inlaat na die hittebron geleë sodat dit die inkomende stikstof voorverhit. Die termiese eienskappe van die rekuperator beïnvloed die dinamiese gedrag van die stelsel. Dit verskil ook van die rekuperator wat in die PBMR aanleg gebruik word, wat 'n kompakte hitteruiler sal wees.

Daar is dus 'n behoefte om 'n hoë-temperatuur hitteruiler vir die PBMM aanleg te ontwerp. Die studie sluit materiaalseleksie en die optimalisering van die voorgestelde hitteruiler se ontwerp in.

'n Wolfram-koper ligering wat uit 68% wolfram en 32 % koper, volgens gewig bestaan, is die voorgestelde materiaal. Die gekose hitteruiler is 'n mini-kanaal hitteruiler wat in 'n teenvloei konfigurasie opgestel is. Die hitteruiler bestaan uit 'n kombinaie van twee lae, een vir die warm vloeier en een vir die koue vloeier, wat mekaar afwissel om die rekuperator te vorm. Dit word dan gehardsoldeer of deur diffusie-hegting geheg om sodoende 'n lekvrye hitteruiler te vorm.

Die finale geometrie is as volg:

- Totale lengte = 0.75 m
- Totale wydte = 0.518 m
- Totale hoogte = 0.8 m

- Aantal kanale wyd = 370
- Aantal warm kanale hoog = 200
- Aantal koue kanale hoog = 200
- Plaat dikte = 1 mm
- Vin dikte = 0.4 mm
- Kanaal hoogte = 1 mm
- Kanaal wydte = 1 mm

Die voorgestelde rekuperator beslaan slegs 10% van die vloer-area en 13% van die volume van die huidige rekuperator. Sy effektiwiteit is 95%, wat 'n styging van 2% in die siklus se effektiwiteit tot gevolg het. Die tyd wat die rekuperator neem tot ewewigstoestand is 25% van die huidige rekuperator se tyd.

ACKNOWLEDGEMENTS

ABBREVIATIONS AND ACRONYMS

a	-	Cell width	[m]
A	-	Area	[m2]
ASME	-	American Society of Mechanical Engineers	
b	-	Cell height	[m]
C	-	Fluid capacity rate	
Cp	-	Specific heat	[kJ/kgK]
CES	-	Cambridge Engineering Selector	
CVD	-	Chemical Vapour Deposition	
D_h	-	Hydraulic diameter	[m]
EES	-	Engineering Equation Solver	
f	-	Fanning friction factor	
h	-	Heat transfer coefficient	[W/m^{2}K]
H	-	Heat exchanger height	[m]
IHX	-	Intermediate heat exchanger	
J	-	Colburn factor	
k	-	Thermal conductivity	[W/mK]
K	-	Secondary losses	
L	-	Length	[m]
LMTD	-	Log Mean Temperature Difference method	
M	-	Material index	
$\dot{m}$	-	Flow rate	[kg/s]
n_h	-	Number of cells high	
n_w	-	Number of cells wide	
NS	-	Nanostructured	
NTU	-	Number of Transferred Units	
Nu	-	Nusselt number	
PBMM	-	Pebble Bed Micro Model	
PBMR	-	Pebble Bed Modular Reactor	
Pr	-	Prandtl number	
q	-	Heat transfer	[W]
R	-	Resistance against heat transfer	
$R"_f$	-	Fouling Factor	
Re	-	Reynolds number	
SiC	-	Silicon carbide	
SS	-	Stainless steel	
t	-	Wall/Fin thickness	[m]
T	-	Temperature	[°C]
UA	-	Overall heat transfer coefficient	
W	-	Heat exchanger width	[m]
WCu	-	Tungsten-copper alloy	
WPIM	-	Weighted Property Index Method	
wt%	-	Weight percentage	
z	-	Inlet velocity head / dynamic pressure	
ε-NTU	-	Effectiveness-NTU method	

Greek symbols

α	-	Heat transfer area density	[m^2/m^3]
ρ	-	Density	[kg/m^3]
ΔP	-	Pressure drop	[kPa]
ΔT	-	Temperature drop	[°C or K]
ε	-	Efficiency	
η_o	-	Overall surface efficiency of a finned surface	
σy	-	Yield strength of the material	
∞	-	Surrounding	

Subscripts

c	-	Cold side
e	-	Outlet
f	-	Fin
ff	-	Free-flow
h	-	Hot side
i	-	Inlet
m	-	Mean
max	-	Maximum
min	-	Minimum
t	-	Total
w	-	Wall

TABLE OF CONTENT

LIST OF FIGURES

LIST OF TABLES

Chapter 1

INTRODUCTION

1.1 BACKGROUND

"The future of mankind is inextricable from nuclear energy. As the world population increases and eventually stabilizes, the demands for energy to assure adequate living conditions will severely tax available resources, especially those of fossil fuels. New and different sources of energy and methods of conversion will have to be explored and brought into practical use. The wise use of nuclear energy, based on understanding of both hazards and benefits, will be required to meet this challenge to existence." (Murray, 2000:XV)

Because of statements like the above, nuclear energy has been recognized as a major alternative for electricity generation, for many years. According to Smith (2000:12/3) it is only since 1973 that substantial research, development and demonstration projects have been undertaken into the application of nuclear power.

The potential for economically competitive fission power cycles is largely dependent on achieving the highest net thermal efficiency. According to Schleicher *et al.* (2000:1) a way of increasing fission power cycle efficiency, is by increasing the effectiveness of the recuperator.

A recuperator is described by The Encyclopaedia of Alternative Energy and Sustainable living (daviddarling website, 2005) as: *"A heat exchanger in which heat is recovered from the product of combustion."*
Efficiency is described as: *"The relationship between potentially usable energy and actually used energy."*
Effectiveness is described as: *"The degree to which a system's features and capabilities meet the user's needs."*

Recuperators in power generating cycles are used to preheat the gas flowing to the core, by extracting the remaining gas energy at the turbine outlet. This concept of heat recovery is used to improve the thermal efficiency of the thermodynamic cycle. An example of a power generation cycle design in which a recuperator is used, is a nuclear reactor with a modular pebble bed reactor.

The Pebble Bed Modular Reactor (PBMR), which is based on the original German design, is one of the projects that are currently underway in South Africa as an alternative to generate electricity. The power conversion cycle of the PBMR is based on a recuperative Brayton cycle with a multi-shaft configuration, (PBMR Website, 2004). Thonon and Breuil (2000:1) claimed that the cycle efficiency of a Brayton cycle is improved by up to 50 %, by athe helium-to-helium recuperator. This indicates that the recuperator is a critical component, and that the efficiency of the cycle is largely dependent on the recuperator.

The Pebble Bed Micro Model (PBMM) was built on the Potchefstroom Campus of the North-West University to test the control system of the intended PBMR and to verify the design results that were generated by the locally developed thermal-fluid network analysis code, Flownex®. A conventional shell-and-tube heat exchanger is employed by the PBMM as recuperator. The PBMM cycle efficiency is only 17%. The current duty for the recuperator is 437kW with an efficiency of 87% (Hasse, 2002:1-23). The material used for the recuperator tube material is AISI 304, with a thermal conductivity of 15-17W/mK.

Increasing the effectiveness of the recuperators for the above cycles is straightforward, but results in a dramatic increase in the recuperator's size and weight, which leads to an increase in cost.

1.2 PURPOSE OF STUDY

The purpose of this study, therefore, is to review methods of improving recuperator efficiency and/or effectiveness, and to employ the most promising methods in designing an improved recuperator for the PBMM.

Chapter 2

LITERATURE STUDY

2.1 BACKGROUND

The literature study will focus on ways of increasing the effectiveness and efficiency of recuperators. Measures that will be used for effectiveness measurements include cost, heat transfer area and overall heat transfer coefficient.

Firstly the generic design methodology for heat exchangers together with ways of increasing the efficiency of heat exchangers will be summarized, as described by Kays & London (1984) and Kakac *et al.* (1981).

2.1.1 Design methodology

The design methodology of a heat exchanger involves a consideration of both the heat transfer rates between the fluids and the mechanical pumping power losses, to overcome fluid friction and moving the fluid through the heat exchanger. The methodology used for arriving at an optimum heat exchanger design is a complex one, not only because of the mathematics involved, but more particularly because of the many qualitative judgements that must be made. This process is an iterative one and is given in schematic fashion in Figure 2.1.

The inputs for the design procedure include, along with the problem statement or specifications, the surface heat transfer, flow-friction design characteristics and information on the physical properties of the working fluids and material used for the recuperator. Trade-off factors may be developed to quantitatively weigh the relative costs of pressure drop, weight and heat transfer performance.

For the sizing of heat exchangers there are two main categories according to Kakac *et al.* (1981). The first is the case where the core geometry, flow rate and entry temperatures

are given. Here the question is, "What is the rating?" That is, what heat transfer rate and effectiveness is predicted and what are the resulting outlet temperatures. The second category is the sizing of the heat exchanger. For this case the flow rates and inlet and outlet temperatures must be given. This will provide the heat transfer rate and effectiveness. If the designer chooses to design a plate-fin heat exchanger, he can select the surface configurations of the fluid sides completely independently. This is one of the advantages of the plate-fin construction.

If the designer selects counterflow conditions for the heat exchanger, only one of the pressure losses (ΔP's) can be prescribed. The other will become a dependent variable. It can only be changed by selecting a different surface for that side. In the case of the cross-flow heat exchanger both of the ΔP's can be prescribed.

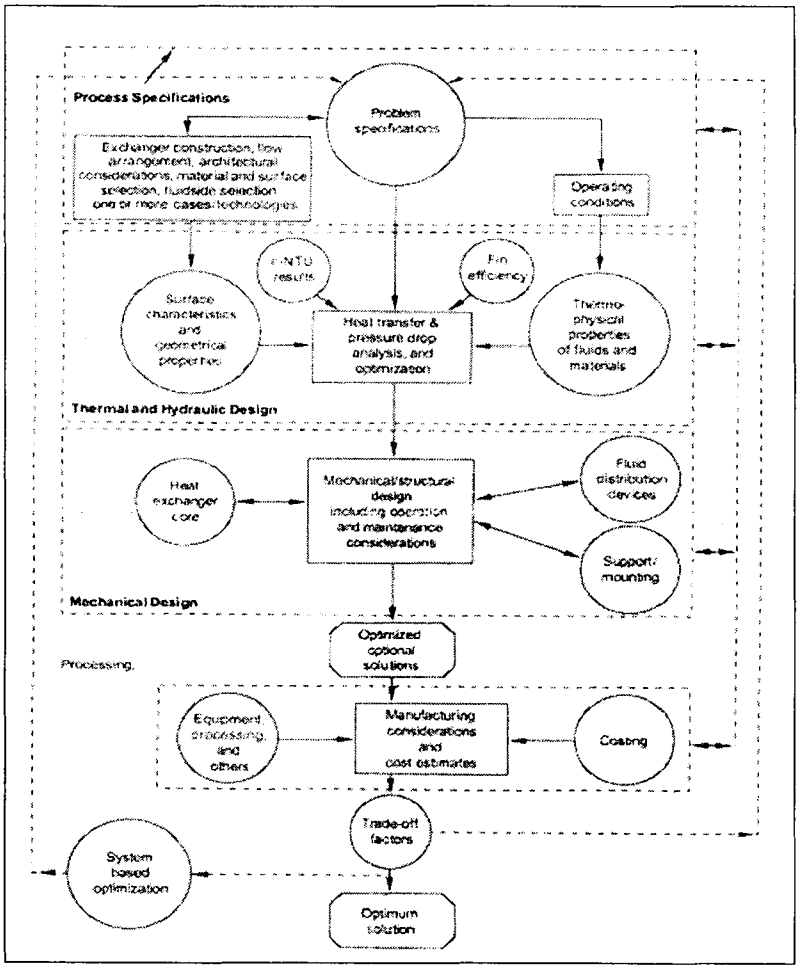

Figure 2.1 Methodology of heat exchanger design and optimization (Kakac *et al.*, 1981).

Some important factors playing a role in designing a heat exchanger with a high effectiveness, according to Kays & London (1984), are as follows:

- For fluids with a high density the heat transfer rates are much higher than the pumping power required. In this case the pressure loss due to friction does not play a controlling role in the design. But in the case of a fluid with a very low density, such as gases, it is very easy to spend more mechanical energy in pumping the fluid than is recovered through heat transfer. Kays & London (1984) claims that mechanical energy, in most thermal power systems, is worth 4 to 10 times as much as the equivalent in heat.

  This suggests that keeping the pressure loss over the heat exchanger as low as possible, is very important for an application where two gases are used.

- As the velocity of the fluid increases the heat transfer rate will also increase. The only problem is that the friction-power expenditure also increases. In the instances of gas-flow heat exchangers, such as the recuperator, the limitations that the friction-power generates force the designer to arrange for moderately low mass velocities. Low mass velocities together with low thermal conductivity of the gasses, relative to liquids, result in low heat transfer rates per unit of surface area. It can be said that compactness lead to higher performance. A compact surface has small passages, and the heat transfer coefficient always vary as a negative power of the hydraulic diameter of the passages.

  This means that the heat exchanger must be as compact as possible. For it to be compact the hydraulic diameters of the flow channels must be as small as possible to maximize the heat transfer area. This must be done in such a way that the pressure loss over the heat exchanger doesn't become too high.

- The effect of longitudinal conduction in the heat exchanger does not play a significant role in the design of a heat exchanger. Conduction through the walls is

much higher than that of the fluid. The only time where it will have an influence is when the flow length is very short and the effectiveness high.

This means that the thermal conductivity of the heat exchanger material has to be as high as possible through the walls. The conductivity in the flow direction of the working fluid and walls do not play a major role.

- Uniformity of flow distribution is the primary function of the headers. Thus, the design objective of headers is to distribute the flow uniformly through the core to minimize the mechanical energy losses. A poorly designed header will result in a lower pressure drop (ΔP) over the core, but the penalty will be paid in the fact that the heat transfer will be much lower. (Kays & London, 1984)

  If the total ΔP is small, say less than 10% of the inlet pressure of the matrix, the header design will not impact greatly on the flow distribution. However, frequently ΔP may be higher than 30% of the matrix inlet pressure, only then does header design become important.

2.2 INCREASING HEAT EXCHANGER EFFECTIVENESS

Literature found on increasing the effectiveness of recuperators is discussed under the following headings:

- The effect of internal flow conditions on recuperator effectiveness.
- The effect of the material selection on recuperator effectiveness.
- The effect of recuperator construction type on recuperator effectiveness.

2.2.1 The effect of internal flow conditions on recuperator effectiveness

Manglik *et al.* (2005) investigated the effect of low Reynolds numbers in forced periodical convection for wavy-plate-fin compact channels. Results highlighted the effect of wavy-fin density on the velocity, temperature fields, the isothermal Fanning friction factor (f) and the Colburn factor (j). The thermal boundary layers on the fin surface were thereby periodically interrupted, resulting in high local heat transfer near the recirculation zones. Increased fin density, however, tended to dampen the recirculation and confine it. The extent of swirl increased with flow rate, when multiple pairs of helical vortices were formed. This significantly enhanced the overall heat transfer coefficient as well as the pressure drop penalty, when it was compared to that of a straight channel with the same cross-section. The relative surface area compactness as measured by the (j/f) performance increases with fin density.

In the study of Sahin (1997), an effectiveness analysis of a recuperator was carried out for obtaining a possible optimum recuperator size. In this analysis, the effect of viscous frictional heating on the recuperator effectiveness was considered. Using the appropriate boundary conditions and solving the governing differential equations, the temperature variations in both streams were obtained. The compressor power required for operation and additional energy needed to raise the fresh air temperature to room temperature were investigated. Then, the effectiveness which could be considered as a function of number of geometrical and flow parameters was optimized. The optimum size of a recuperator was obtained analytically and the parameters that have an effect on the size of the recuperator studied. Sahin (1997) concluded that:

- The viscous frictional heating reduced the recuperator effectiveness.
- An optimum size can be obtained, in which the thermal effectiveness becomes a maximum. This optimum size depends on the viscosity of running fluids.
- A limiting value of NTU (maximum size of recuperator) can be found such that the effectiveness drops to zero.

Minhas & Lock (1996) investigated the effect of the Prandtl number on the heat transfer characteristics of a bayonet tube. The Reynolds number was varied over the laminar and transitional range 350< Re <2625. They found that the Prandtl number has a significant influence on the heat transfer rate, especially in the laminar regime. The Prandtl number decreased the thermal boundary layer on the outer tube if the Prandtl number is increased, which contributed to an increase in heat transfer.

Manglik & Bergles (1995) investigated the influence of offset strip fins on heat transfer and pressure drop. They included the transition region between laminar and turbulent flow in their study. A suggested arrangement, to improve heat transfer rates, considered a large enough offset to put successive fins out of the wakes of their immediate upstream neighbours. The heat transfer and friction factor data for 18 offset strip fin surfaces had been analyzed and were shown to be affected by the fin geometric parameters along with the Reynolds number. In the absence of quantitative data, no definite design recommendations could be made.

The paper by Zhu & Zhang (2004), discussed an integrated optimal design of the materials, placement, size and flow-rate of a plate heat exchanger. The paper also illustrated how the placement of flow channels influence the heat transfer area. By optimizing the design, plate heat exchangers will effectively be smaller, which will lead to a reduction in cost of the heat exchanger. Titanium was selected as the material for this recuperator, as it has the necessary resistance to high chloride concentrations. The two arrangements used for the plates were lambdoidal and straight. The operating pressure of the lambdoidal arrangement exceeded 1.0 MPa, while that of the straight model was about 1.0 MPa. In addition, the heat transfer coefficient and pressure drop of the lambdoidal arrangement were both higher than that of the straight model. Zhu & Zhang (2004) concluded that the flow velocity influenced both heat transfer efficiency and pressure drop. They found that the higher the flow-rate of the circulating water, the smaller the heat transfer area needed to achieve the same efficiency. A problem identified was that for a higher flow-rate, the pressure drop increased.

The thermal performance of pin-fin assemblies, for in-line and staggered configurations, was investigated experimentally by Babus'Haq et al. (1995). The materials used for the pin-fins were an aluminium alloy (k = 168 W/mK), mild steel (k = 54 W/mK) and polytetrafluoroethene (k = 1.7 W/mK). They found that the staggered configuration yielded a higher steady-state heat transfer rate than the in-line configuration, when both were under similar conditions and for an equal number of pin-fins. The optimal separation between the pin-fins in the streamwise direction, corresponding to the maximum rate of steady-state heat transfer from the assembly, increased as the thermal conductivity of the pin-fin material increased. The optimal separations in the spanwise direction remained invariant. The overall pressure drop along the heat exchanger for all tested configurations was found to increase steadily with increasing mean inlet velocities and with decreasing uniform pin-fin spacing.

Herman & Kang (2002) visualized unsteady temperature fields in the grooved channel with curved vanes using holographic interferometry. The heat transfer performance of the investigated channel was compared with that of the basic grooved channel. The addition of curved vanes above the downstream end of the heated block redirects the flow from the main channel into the groove. Heat transfer shows an increase by a factor of 1.5–3.5, when compared to the basic grooved channel, mainly due to increased flow velocities in the groove region. Flow transition from steady to oscillatory occurred around Re = 450 and flow oscillations contributed to heat transfer enhancement. The pressure drop was 3–5 times higher than in the basic grooved channel.

Wang et al. (1999) presented a paper on a gas-to-gas heat exchanger with strip fins. The heat exchanger design and construction were based on a method sealing rectangular strip fins in slots in opposite walls of a rectangular pipe. Fins were fixed and sealed to the walls simultaneously by high temperature brazing of glass mixed with metals in a furnace. The additional advantage of glass was that it formed a coating on the heat transfer surface to protect the surface from corrosion. A number of measurements were carried out to test the performance of the heat exchanger. The results measured indicated that the heat transfer coefficient and pressure drop increased with the ratio of heat transfer

area to volume (fin density). From the point of pumping power per unit heat transfer surface area, high density displayed high performance. In the higher Reynolds number region, whistle happened and caused a higher friction factor.

O'Doherty et al. (2001) considered the assessment and analysis of heat transfer enhancement devices which could be taken into account for a bayonet tube heat exchanger. Due to restraining conditions, such as material selection and manufacturing complexity, simple rib roughened surfaces in the form of rings were used on the air side flow, in the annulus. Analysis of the effect of the rings was studied, starting from cited geometries, using computational fluid dynamics. Validation was carried out using laser diagnostics. For the range of Reynolds numbers (Re_{ave} =160,000) considered, the optimal ring configuration was a ring to annulus height ratio of 0.37 with a pitch to ring height ratio of 10. This proved to be the optimal heat flux to pressure drop ratio for the given conditions. This resulted in a predicted enhancement from 230 to 650 kW/m^2 heat flux, but at the expense of an increased pressure drop by a factor of around 12.

2.2.2 The effect of the material selection on recuperator effectiveness

In his work, McDonald (2003), looked for methods of increasing the effectiveness of microturbines. One of the methods he explored was by increasing the temperature in the cycle. A problem he experienced with increasing the temperature in the cycle was that the materials had to be able to cope with this higher temperature. Table 2.1 is a list of the materials selected by McDonald (2003) as the materials to be used at the various temperatures. He claimed that ceramic materials could be the key to higher temperatures and higher efficiencies for microturbines. A bi-metal recuperator was proposed in order to reduce the cost of recuperators. By using a bi-metal recuperator it is possible to use a cheaper material for the low temperature region and the more expensive material only for the section with the higher temperature.

Table 2.1 Heat exchanger materials at different temperatures

Temperature	Material used	Composition
650°C	347 SS	Fe-68%; Cr-17%; Ni-11%; C-8%; Mn-2%; Si-1%.
750°C	347 SS	Fe-68%; Cr-17%; Ni-11%; C-8%; Mn-2%; Si-1%.
800°C	Inconel/ 625	Ni-62%; Cr-21%; Mo-9%; Fe-5%; Nb+Ta-3.5%; Co-1%.
850°C	Haynes 230	Ni-57%; Cr-22%; W-15%; Co-5%; Fe-3%; Mo-2%; Mn-0.5%; Si-0.4%; Al-0.3%; C-0.1%; La-0.02%; Br-0.015%
900°C	Haynes 214	Ni-75%; Cr-16%; Al-4.5%; Fe-3%; Mn-0.5%; Si-0.2%; Zr-0.1%; C-0.05%; B-0.01%; Y-0.01%

In their paper Natesan *et al.*(2003) Fe-Cr-Ni alloys such as Alloy 800H and austenitic stainless steels were considered for recuperators and reactor internals, while nickel-based alloys such as 617, Hastelloy X, and Hastelloy XR were considered for components that are exposed to the helium coolant at temperatures of up to 900°C. Figure 2.2 illustrates how the thermal efficiency of a microturbine increases as the turbine inlet temperature increases. Also on Figure 2.2 are the different materials used at these temperatures. The selection of these materials is primarily based on material strength at high temperatures.

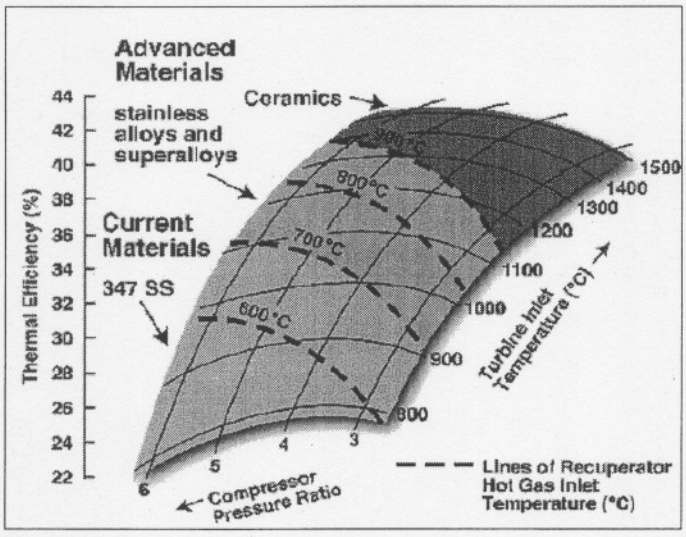

Figure 2.2 The influence of recuperator materials on thermal efficiency (Natesan *et al.*, 2003)

A novel type of high temperature heat exchanger was presented by Luzzatto et al. (1997), where the main heat transfer parts were made from CMC (Ceramic Matrix Composite) materials. The CMC material used was a particles reinforcing phase-based material,

SiC_p/Al_2O_3. The heat exchanger was based on a modular concept and could handle very high temperatures and pressures. The design was performed by means of computer codes, such as the COHEX code (developed ad hoc), ANSYS and RECUP, to validate some of the results presented. This design:

- Reduced the total volume-to-surface ratio of the heat exchanger.
- Overcame some material manufacturing limitations such as size of components, number of seals and differential thermal expansions.
- Showed smaller brittleness, higher toughness, corrosion and creep resistance, less harmful failures, with respect to designs based on monolithic materials. It also exhibited better reliability and durability.

The main focus of the study by Seong *et al.* (2000) was high temperature corrosion in steel mills. According to Seong *et al.* (2000) ferritic stainless steels are the preferred choice as recuperator material for steel mill recuperators, as their thermal expansion and heat transfer properties are better than those of austenitic stainless steels. They found that for applications where the temperature was above 900°C, Silicon Carbide (SiC) was used as pipe material for the recuperators. To improve the service life of the recuperator pipes, Seong et al. (2000) evaluated several protective metal coatings. The coatings investigated were cobalt - (10095) and nickel-based (13017 & 16801). These coatings can protect the base material against hot corrosion, erosion and abrasion. Test results showed that coatings with high chromium content, either as a form of carbide or as an alloying element, had excellent corrosion resistance. As a form of carbide, the Cr_3C_2-NiCr coatings, sprayed by the HVOF (High Velocity Oxygen Fuel) thermal spray process, and as an alloying metal, the 45CT coating were recommended as a promising coating for heat exchanger pipes used in steel mills. Seong et al. (2000) even recommended these coatings to be used in cases where molten salt corrosion attack is experienced.

Boomsma *et al.* (2003) discussed the use of metal foams as compact heat exchangers. Open-cell metal foams with an average cell diameter of 2.3 mm were manufactured from 6101-T6 aluminum alloy and were compressed and fashioned into compact heat

exchangers measuring 40mm x 40 mm x 2.0 mm high, possessing a surface area to volume ratio of 10 000m^2/m^3. They were placed into a forced convection arrangement using water as the coolant. These experiments performed with water were scaled to estimate the heat exchangers' performance when used with a 50% water–ethylene glycol solution, and were then compared to the performance of commercially available heat exchangers which were designed for the same heat transfer application. The heat exchangers were compared on the basis of required pumping power versus thermal resistance. It was found that the compressed open-cell aluminum foam heat exchangers generated thermal resistances that were two to three times lower than the best commercially available heat exchanger tested, while requiring the same pumping power.

The work of Tadrist *et al.* (2004) illustrated the advantages of using fibrous materials in heat exchangers. They also investigated the impact of local structure of the solid matrix over transport properties. Fibrous materials present unique characteristics, which lead to a strong increase of thermal performances without adding much pressure drop.

The use of such a metallic matrix in channels had the following outcomes:

- Convective boiling.
- An increase in heat transfer.
- Very low superheat.
- Higher critical heat flux than for regular tubes.

These metallic structures presented interesting mechanical properties, high surface-area density and are easily manufactured. Because of these properties they could be used to simultaneously increase thermal efficiency and participate in added strength in the mechanical design of heat exchangers, leading to higher compactness and manufacturing cost savings.

Maziasz *et al.* (2003) investigated materials to be used at 650°C, 700°C and 760°C. Their objective was to work with recuperator manufacturers and commercial suppliers of foil and thin sheets. This was done in order to enable manufacture and evaluation of upgraded recuperators from cost effective alloys with improved performance and

temperature capability. Oxidation/corrosion testing at 650°C in 10% water vapour indicated very severe attack on AISI 347 steel after only a few thousand hours. This indicated that alloys with significantly better properties were needed for temperatures ranging from 650°C and higher. Maziasz *et al.* (2003) suggested the use of AL347HP (AISI 347 modified by ORNL and Allegheny-Ludlum Technical Center) as material for temperatures up to 704°C (1300°F). The recommended materials to use at 760°C (1400°F), or higher, included foils of HR120 (from Elgiloy Specialty Metals) and Alloy NF709 (20Cr/25Ni, Nb, N).

2.2.3 The effect of recuperator construction type on recuperator effectiveness

Traverso & Massardo (2005) presented a new approach for the optimization of microtubine recuperators from a technical and economical point of view. The procedure proposed has been implemented in software called CHEOPE (Compact Heat Exchanger Optimization and Performance Evaluation). Types of recuperator constructions considered were brazed plate-fin and welded primary surface recuperators. The method used was based on achieving the following outcomes:

- Best compactness.
- Minimum cost.
- Nominal total pressure drop.

Traverso & Massardo (2005) presented equations for the determination of minimum plate thickness. With the use of these equations they claimed to have improved the compactness of recuperators more efficiently. Results of the study showed that the primary surface recuperator was the best choice for microturbine applications. This is mainly due to the fact that the primary surface recuperators were able to combine high heat exchanger effectiveness and smaller volumes, which also caused a decrease in the weight of the recuperator. According to Traverso & Massardo (2005) the lower compactness and higher material requirements of the plate-fin concept, are mainly related to the lower heat transfer effectiveness of the secondary surfaces. This lower

effectiveness of the secondary surfaces caused the heat exchanger to require more heat transfer surface for the same design-performance specification. CHEOPE was shown to be able to identify plate-fin recuperator designs with a cost reduction of up to 20%, when the least expensive solutions are compared to the most compact designs. It was found that, the higher the effectiveness and the size, the higher the potential reduction in cost given by the optimization. For the most cost-effective plate-fin recuperators, the specific capital costs ranged from 125$/kW to 190$/kW (R840.00 to R1276.80, if 1$ is taken as R6.72 as 23 June 2005), depending on the effectiveness required and the size of the plant. In all the case studies presented in this paper of Traverso & Massardo, primary surface recuperators were shown to be able to decrease the volume and the material weight by 50% or more when compared to an equivalent plate-fin heat exchanger. This in turn implied an even higher potential for cost reduction due the simpler and cheaper production process.

Whyatt (2003) used a micro-channel recuperator for his design. As the flow rate was very low for this design, this was the ideal construction. The material used was the nickel-based alloy, Inconel 600. Flow channels were photo-chemically etched into the sheets, after which the plates were diffusion bonded. This increased the heat transfer area and lead to a more compact design, which had a significant decrease in the material costs.

Boman & Doty (2002) presented heat exchangers operating under laminar conditions, even at high levels of power and flow. This was achieved by using hundreds (or thousands) of parallel micro-tubes. This type of heat exchanger construction is also known as a micro-tube strip heat exchanger. The results of the study showed good performance with a factor-of-four increase in specific conductance (heat-exchange power per mass per LMTD, W/kg K) relative to comparable compact designs with high effectiveness. According to Boman & Doty (2002), the effectiveness that was achieved in this study, still falls slightly below the calculated theoretical effectiveness.

In the second part of their paper, Thonon & Breuil (2000) made a selection of candidate heat exchanger constructions to be applied as recuperator operating at high temperatures,

maximum temperature above 500°C. This selection was based on their capabilities to cope with the operating conditions parameters (pressure, temperature and flow rate) and other parameters such as fouling, corrosion, compactness, weight, maintenance and reliability. Within the high temperature reactor context and due to the high pressure difference for the recuperator, only welded, brazed or diffusion bonded heat exchangers were suggested. Diffusion bonded heat exchangers with micro-channels appeared to be the most promising concept for recuperator applications. In spite of a more important pressure drop, this concept was rated as the best, in particular in terms of reliability, mechanical resistance and compactness. This concept has been proposed as alternative solution to the frame of the GT-MHR and PBMR projects.

Yan *et al.* (2003) introduced overall objectives of the GTHTR300 power plant program and described the plant design and development approach taken to achieve their goals. The GTHTR300 power plant program is a design and developmental program for the gas turbine high temperature reactor with 300MWe nominal-capacity undertaken by the Japan Atomic Energy Research Institute. The first approach that was used to lower the recuperator cost is minimization of weight and volume, given the thermal duty specified for the cycle design. The fact that both sides of the recuperator operate in non-corrosive and non-erosive helium, permitted the use of an extremely compact plate-fin surface. For a fixed heat transfer duty and effectiveness, the weight and volume of recuperator depended heavily on the selection of fin compactness. This meant that the fin geometry (fin height and fin pitch) used, had to be as small as practical in fabrication. The recuperator design selected a fin size of 1.2mm height by 1.2mm pitch as the optimum dimensions.

Esbeck *et al.* (1997) gave an annual ATS (Advanced Turbine Systems) report that was required from Solar Turbines Incorporated under contract for the development of the Mercury 50. Solar's proven primary surface recuperator construction was used. The construction was rugged and the modular nature of the design gave it superior flexibility to handle thermal stresses. Air cells were constructed from 0.004 inch thick sheets made of AISI 347 stainless steel folded into a corrugated pattern. This folded shape maximized

the primary surface area that is in contact with the working fluids. Clamping the cells rather than welding them to one another allowed the assembly to flex freely to relieve stresses, rather than concentrating stresses at the weld locations. The primary surface recuperators were significantly smaller and lighter than competing technologies, had superior performance, improved reliability and could easily accommodate the thermal transients associated with start-ups, shutdowns and full-load transients during turbine operation. The primary surface recuperator presented provided a high efficiency of more than 90%, with moderate pressure drop and a long life as demanded by industrial turbine applications.

2.3 SUMMARY

The focus of the literature study was to identify different methods of increasing the effectiveness of recuperators.

It was found that there are many methods of increasing the effectiveness. For this study these methods were divided into three categories namely:

- Improving internal flow conditions.
- Optimizing the material selection for recuperator.
- Recuperator construction type used.

Improving internal flow conditions mainly consisted of methods which added secondary surfaces like fins or fibrous materials in the flow passages. These fins increase the heat transfer area, which will increase the amount of heat that is transferred. Thus the higher the fin density the higher amount of heat transferred. Increasing the heat transfer area will lead to a more compact recuperator which will be smaller for the same duty and be less expensive. A disadvantage of adding fins is that as the fin density increases, so will the pressure loss over the core. The effect of varying different flow properties was also investigated, but as the properties are usually predetermined by the cycle, it is very difficult to implement these methods.

Secondly materials and material selection methods used for recuperators were investigated. The aim of all the material selection processes found was to minimize the cost of the material. From the reviewed articles it is clear that materials used in recuperators are standardized and that only certain proven materials are used. The choice of material mainly depends on the maximum working temperature and type of working fluid (consideration of corrosion). For maximum working temperature the most important properties taken into account are the high temperature strength, creep and high temperature corrosion. A way of improving corrosion resistance of materials according to literature found was by applying a coating of a corrosion resistant material on the surface of the base material.

Recuperator construction type was found to be a very important aspect of increasing the effectiveness of a recuperator. It is clear that certain construction types are much more compact than others and therefore more effective. The recuperator construction type used mainly depends on the specific requirements of the cycle in which it is implemented and has to be considered before any design can be finalised.

An aspect that was found to be neglected during the material selection process of recuperators was the consideration of thermal conductivity at the working temperature of materials during the material selection process of recuperators. For low temperature heat exchangers copper is the favourite material used because of its very high thermal conductivity, about 390 W/mK at room temperature, and relatively low cost. It is only the decrease in strength of copper at high temperatures which makes it unsuitable for use if high pressures are experienced. Materials generally used for high temperature recuperators have a thermal conductivity of lower than 40 W/mK at operating temperature (500-1000°C). This is nearly 10 times lower than that of copper.

For this reason the main focus of this study was to conduct a complete material selection for materials to be used for high temperature recuperators. The chosen material and other ways of increasing the efficiency of a recuperator, which was found in the literature, will

then were applied to design an improved recuperator to be employed in the PBMM, which is situated at the Potchefstroom Campus of the North-West University.

Chapter 3

MATERIAL SELECTION PROCESS

3.1 INTRODUCTION

As seen in Chapter 2, certain materials are commonly used for the manufacturing of recuperators. These materials are selected according to the specific demands of the operational conditions in which the recuperator is employed.

To select a material it is firstly necessary to determine the attributes to which a suitable material has to comply. Properties such as thermal conductivity and specific heat all play an important role in achieving an optimum design. Other factors such as price of material and manufacturing process, and manufacturability will also determine the choice of material.

3.2 ENGINEERING ANALYSIS

A suitable material has to comply with certain requirements that are set by the operating conditions of the cycle in which the recuperator is employed. For this study the material selection is based on the PBMM cycle.

Table 3.1 gives the inlet conditions for the recuperator, which is employed in the PBMM cycle, for both sides. The maximum temperature and pressure that is experienced by the recuperator is 527.7°C and 805kPa respectively. The pressure difference (ΔP) between the two sides is 547.3kPa. It is necessary that the chosen material has adequate strength at the working temperature to be able to cope with this ΔP. To minimize thermal stress, which is caused by the difference in temperature, a material with minimal thermal expansion and thermal fatigue would be preferred.

Table 3.1 Inlet properties for the recuperator in the PBMM cycle (Hasse, 2002).

Low Pressure side		
Mass flow rate	1.148	kg/s
Inlet Pressure	257.7	kPa
Inlet Temperature	527.7	°C
High Pressure side		
Mass flow rate	1.086	kg/s
Inlet Pressure	805	kPa
Inlet Temperature	95.3	°C

According to the literature study the most effective recuperator is one with a maximum heat transfer area. This can be achieved by using very small flow channels of an infinite number. In order for the channels to be small, in the range of 0.001mm, the channels have to be machined very finely or etched into the plates. Joining of the plates to each other with the use of brazing, welding or diffusion bonding is a must for a leak-tight recuperator.

As is the case in most designs, cost also plays an important role in the selection of the material.

3.3 SELECTION STRATEGY

The strategy followed in the selection of an appropriate material was summarized as followed by Ashby (1999).

- Determining the function, objective and constraints of the design.
- Consider all materials as a candidate material untill proven otherwise.
- Screening, eliminating those that lack the required design attributes.
- Ranking those which remain, using material indexes.
- Apply a decision matrix to determine whether the material is practical.
- Seeking support information for the top candidates.
- Making a final choice.

Figure 3.1 will be considered a simplification of the recuperator for illustration purposes. As mentioned, the first step is to determine the function, objective and constraints of the design. Table 3.2 gives the function, objective and constraints of the recuperator.

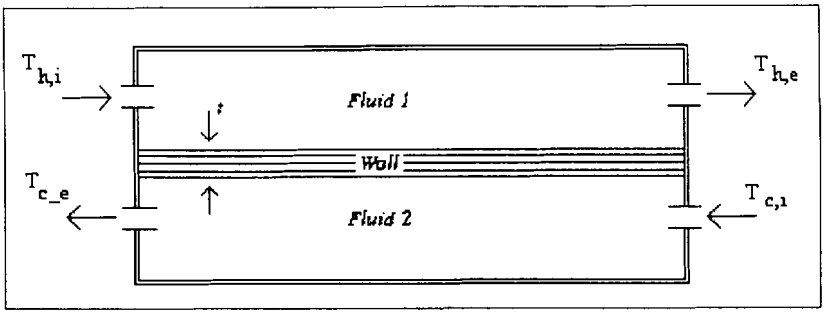

Figure 3.1 Illustration of a simple plate heat exchanger.

Table 3.2 Design requirements for the recuperator material

Function	The Primary function of a heat exchanger is to transfer heat from fluid 1 to fluid 2.
Objective	To maximize the heat flux per unit area exposed to the fluid with no failure under ΔP.
Constraint	(a) Mustn't fail at the working temperature of 527.7°C (801 K).
	(b) Must be thermal shock resistant.
	(c) Mustn't fail due to corrosion because of the working fluid, nitrogen.
	(d) Must be available in plate form or be able to adapt the desired form.
	(e) Cost as low as possible

Screening was done by plotting graphs with properties against each other to eliminate the materials that will not be able to operate at these conditions. All available materials are considered by using the material databases that are available. For this study, Cambridge Engineering Selector (CES) Version 3.1 was used. More information on all of the candidate materials were then searched for, to determine whether the solution would be realistic or not. This search led to the discovery of other candidate materials, not considered in the CES data base. The main consideration for these other candidate materials was their very high thermal conductivity.

Ranking is done by determining a material index (M) to which the material has to comply. A material index is a group of properties that, if maximized, maximize some aspect of the performance of the component.

The results were then sorted into an order ranging from the best to the not so good choice of material with the help of the decision matrix method. Only after this whole process a well informed final decision was made on the best material for the recuperator.

3.3.1 Selection

Screening was done with the assistance of the constraints as indicated in Table 3.2.

To comply with these constraints graphs were plotted for:

- Maximum service temperatures vs. Price
- Materials vs. Shape (Plate)
- Hardness vs. Materials
- Thermal conductivity vs. Materials

All graphs were drawn by using the database Cambridge Engineering Selector (CES). See Figures 3.2-3.5.

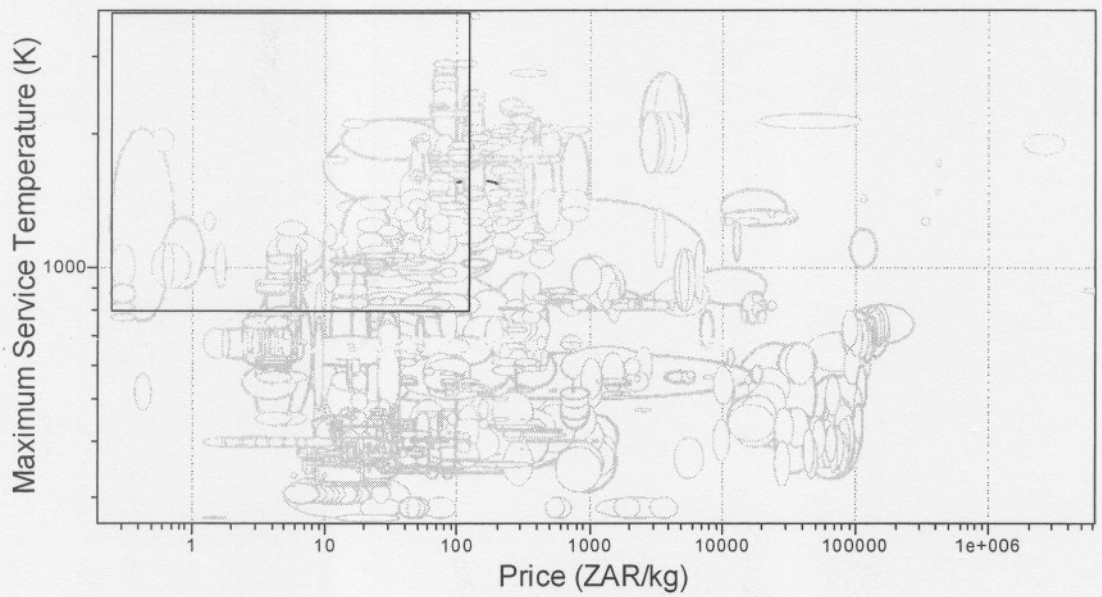

Figure 3.2 Maximum service temperatures vs. Price.

For the plot in Figure 3.2 the limit for the maximum service temperature was set at temperatures higher than 800K. The price was neglected at first to get the best possible materials. Later the limit was lowered to get a more cost-effective material.

In the plot, shown in Figure 3.3, different materials were plotted against available shape. The shape required for the material of the recuperator is plate form.

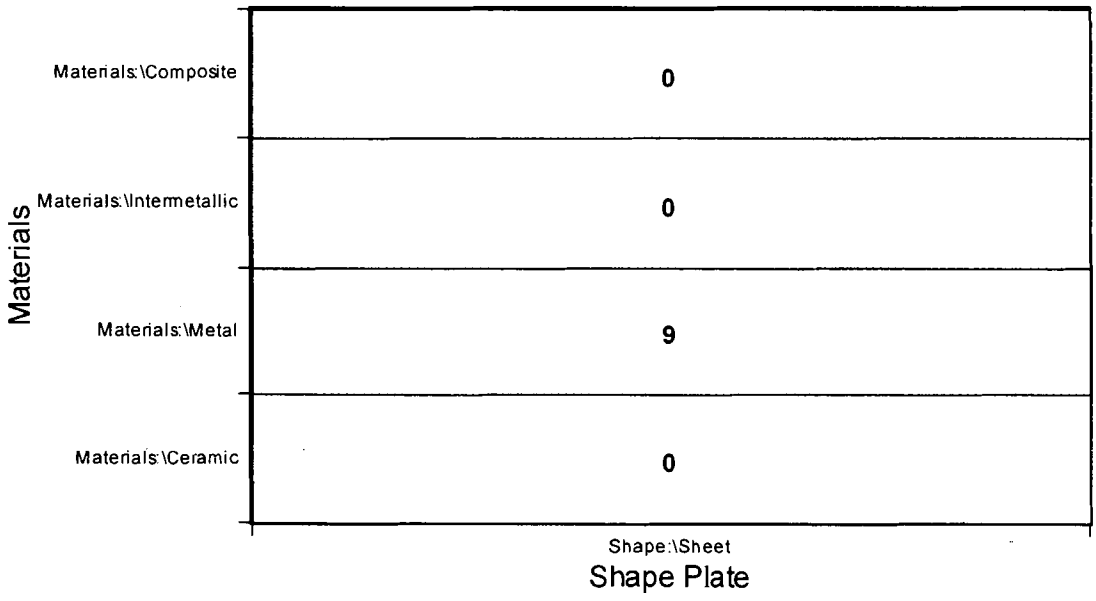

Figure 3.3 Materials vs. Shape (Plate).

In order to shape and machine the material, the material must not be too hard. Figure 3.4 shows a plot of hardness ranges for the materials. This was used to eliminate the materials which are too hard to machine.

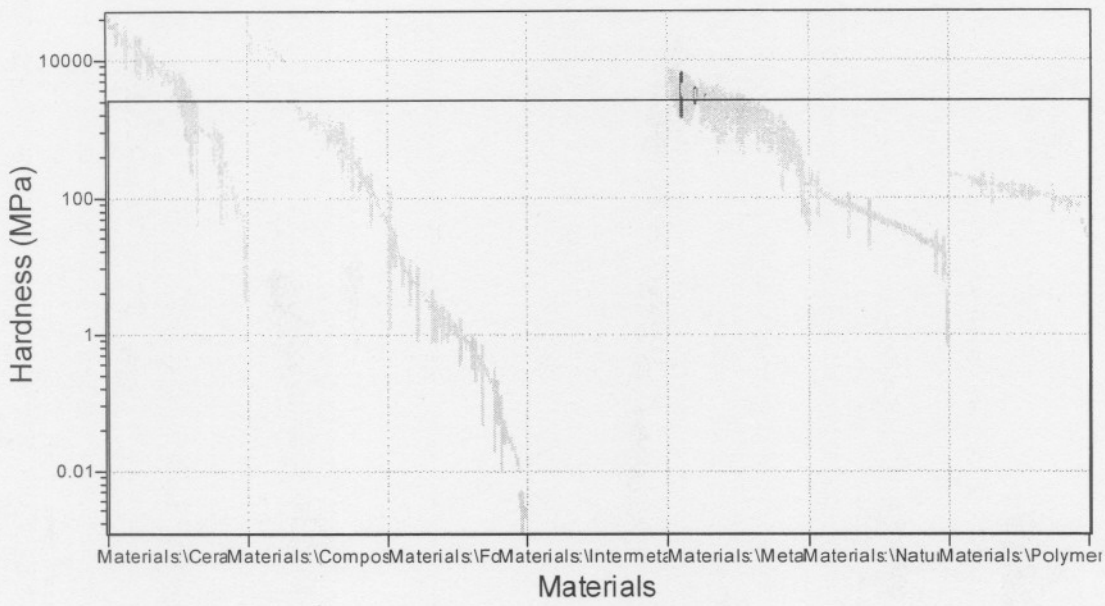

Figure 3.4 Hardness vs. Materials

Thermal conductivity is the measure of ability to transfer heat through the material. A suitable material for the recuperator must transfer as much heat as possible. For this reason thermal conductivity was plotted against the material. See Figure 3.5 for this graph.

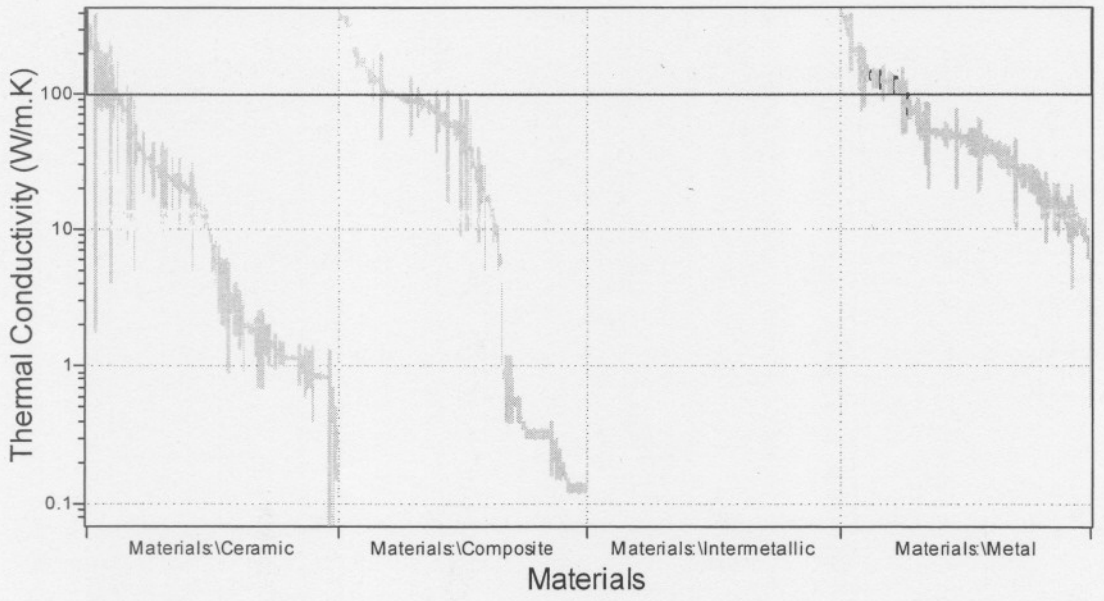

Figure 3.5 Thermal conductivity vs. Materials

After screening, ranking was done. Ranking is done with the use of material indices.

Because the material index is independent of the geometry, tubular geometry will be considered for the deviation of the material index for this recuperator. As stated in Table 3.2 the main objective in this selection is to maximize the heat flux per unit area exposed to the fluid with no failure under ΔP. Heat flux is expressed as:

$$q = -k\frac{\Delta T}{t} \tag{3.1}$$

With: q = Heat flux

k = Thermal conductivity

$\Delta T = T_1 - T_2$

t = Wall thickness

Strength to withstand ΔP is expressed as:

$$\sigma = \frac{\Delta P \cdot r}{t} \leq \sigma_y \tag{3.2}$$

With: $\sigma \leq \sigma y$ (Because the maximum stress allowed has to be lower than the yield strength of the material)

ΔP = Pressure difference between the primary and secondary sides.

r = Radius of the tubes.

This is then written as:

$$t = \frac{\Delta P \cdot r}{\sigma_y} \tag{3.3}$$

If this equation is substituted in equation (3.1) to eliminate t, equation (3.1) becomes:

$$q = -\frac{\Delta T}{\Delta P \cdot r}\left(k \cdot \sigma_y\right) \tag{3.4}$$

The material index (M) is the part of equation (3.4) with all the material properties:

$$M_1 = k\sigma_y \tag{3.5}$$

To maximize q the material index must be maximized.

In order to plot a graph illustrating this selection, the index was written in the form y=mx+c. This was done as follows:

$$M_1 = k\sigma_y \tag{3.5}$$

Written in log form, equation 3.5 is written as:

$$\log M_1 = \log k + \log \sigma_y \tag{3.6}$$

$$\log \sigma_y = -\log k + \log M_1 \tag{3.6.1}$$

Figure 3.6 shows the graph for M_1.

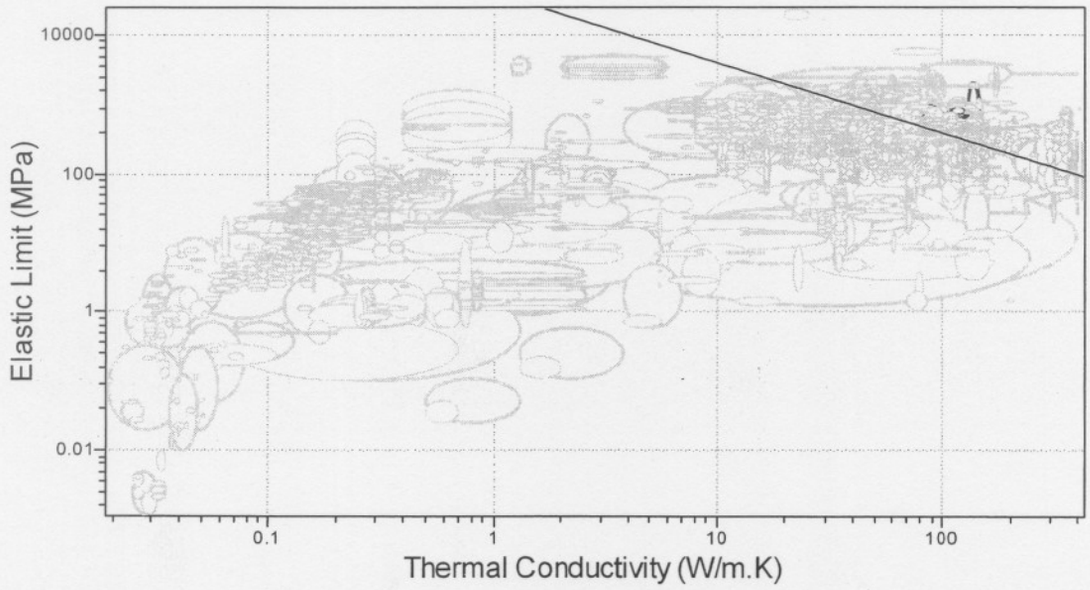

Figure 3.6 Elastic limit vs. Thermal Conductivity

Another constraint for the recuperator is that the material must be thermal shock resistant. A material index was determined for this constraint as followed. Firstly the deformation (ε) of a material was considered. This is expressed as follows:

$$\varepsilon = \sigma_y / E \tag{3.7}$$

where E = Young's modulus

The deformation of a material due to a change in temperature is expressed as:

$$\varepsilon = \alpha \Delta T \tag{3.8}$$

where α = thermal expansion

By substituting deformation in equation 3.7 with equation 3.8, equation 3.7 can be written as:

$$\sigma_y / E = \alpha \Delta T \tag{3.9}$$

In order to determine the material index, all the material properties must be grouped. If this is done equation 3.9 is written as:

$$\Delta T = \sigma_y / E\alpha \tag{3.10}$$

Thus the material index is:

$$M_2 = \sigma_y / E\alpha \tag{3.11}$$

In order to plot a graph illustrating this selection, the index was writtien in the form y=mx+c. This was done as follows:

$$M_2 = \sigma_y / E\alpha \tag{3.11}$$

Written in log form, equation 3.11 is written as:

$$\log M_2 = \log \sigma_y - \log E\alpha \tag{3.12}$$

$$\log \sigma_y = \log E\alpha + \log M_2 \tag{3.12.1}$$

Figure 3.7 shows the graph for M_2.

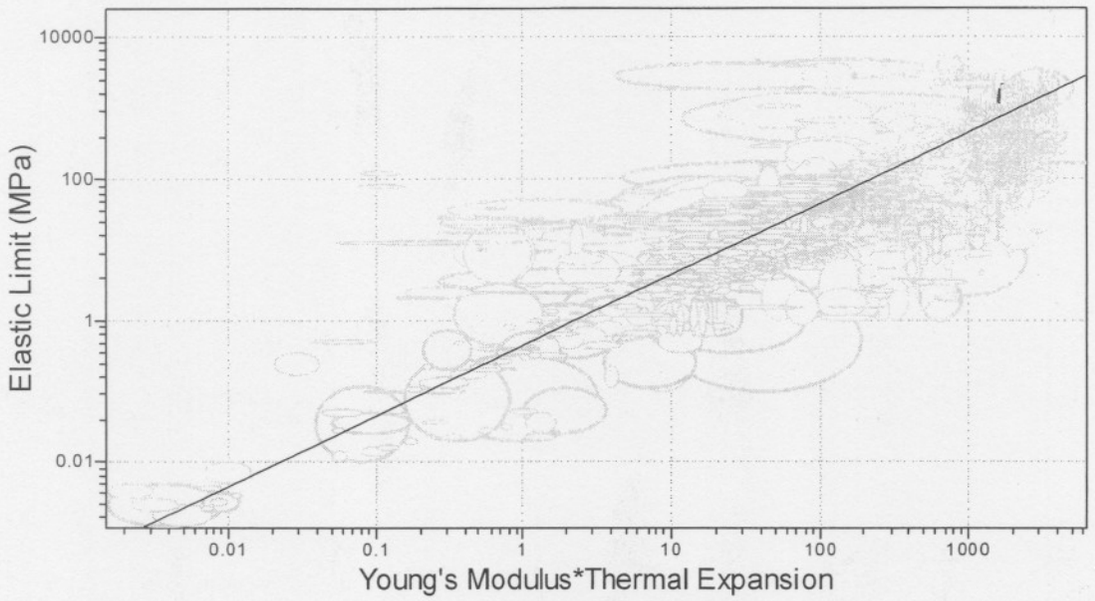

Figure 3.7 Elastic limit vs. Young's Modulus*Thermal Expansion

After screening and ranking was carried out, a number of materials were considered as possible candidate materials for the recuperator. Table 3.3 is a list of these candidate materials from the database CES.

Table 3.3 List of candidate materials after screening and ranking

Molybdenum Alloy 362 (Mo-0.5Ti alloy)
Molybdenum Alloy 363 (TZM Alloy)
Molybdenum Alloy 366 (Mo-30W alloy)
Molybdenum Titanium Alloy
Molybdenum Tungsten Alloy
Molybdenum, Commercial Purity
Tungsten - ASTM Class 1 (90%W)
Tungsten - ASTM Class 4 (97%W)
Tungsten-10%Copper alloy, "Elkonite 50W3"

3.4 EVALUATION OF CANDIDATE MATERIALS

During the evaluation process, more information on the candidate materials was gathered in order to see whether the materials comply with the restrictions and could be used for the application. The evaluation of the candidate materials will be discussed in the following section.

3.4.1 Tungsten and tungsten alloys

3.4.1.1 Pure Tungsten

Tungsten is mostly used for its excellent high temperature properties. High hardness, 4500-5300 MPa (CES, 2000), and strength, 1350-1680 MPa (CES, 2000), makes it highly resistant to mechanical wear, (Lassner & Schubert, 1998).

Tungsten could be shaped by hot rolling at a temperature between 1600 and 1650°C (High-density Tungsten based materials, 2005).

Tungsten has the highest melting point and lowest vapour pressure of all metals, and at temperatures over 1650°C has the highest tensile strength. Because of its very high melting point, 3410°C, the temperature at which tungsten has to be sintered is very high. To sinter, tungsten must be kept at a temperature between 2700 and 3000°C, (Lassner & Schubert, 1998).

Pure tungsten was chosen by the Weighted Property Index Method (WPIM) as a possible material because of is very high elastic limit (1350-1680 MPa) (CES, 2000) and relatively high thermal conductivity (170-175 W/mK) (CES, 2000). Tungsten has high temperature stability with a low thermal expansion with a value between 4.2-4.4 μm/K (CES, 2000).

3.4.1.2 Tungsten-Copper alloys (WCu)

WCu are materials that combine the thermal properties of copper with the high temperature properties of tungsten. Tungsten is the main component of these alloys and the reason for their high density (between 17 and 18.5 g/cm^3) (Lassner & Schubert, 1998). WCu is not a real alloy in the strict sense of the word, because the mutual solubility of the components is practically zero. The copper serves as binder matrix, which holds the brittle tungsten grains together and which makes the alloys ductile and easy to machine. It is therefore called a pseudoalloy.

In the literature consulted, it was found that there are different methods of producing WCu. According to most of the literature on manufacturing of WCu found, the porosity of the final product seems to play an important role in achieving maximum thermal conductivity. This means that the aim is to achieve maximum density and the lowest porosity for the specific WCu.

The methods achieving densities of more than 98% of the theoretical, for WCu composites with copper content 5-40 wt%, according to the literature found are:

- Mechano-thermochemical process, Hong & Kim (2003).
- Sintering under ultra-high pressure, Zhou & Kwon (2005).
- Thermo-mechanical method, Li *et al.* (2003).
- Nanostructured powders that was prepared by mechanical alloying. The compacted specimens were then sintered at temperatures in the range 1000-1300°C, Kim & Moon (1998).
- Nanocomposite powder that was fabricated using Tungsten and CuO powder with the ball-milling and hydrogen-reduction process. Then it was sintered at 1200°C, Kim *et al.* (2004).
- Infiltration of a porous tungsten structure, Lassner &, Schubert (1998).

As high performance materials, WCu alloys/composites are characterized by high thermal conductivity, low thermal expansion and high wear resistance combined with excellent electrical conductivity.

Both elements of these materials are very good conductors of temperature. High conductivity copper has a thermal conductivity of 391 W/mK (Matweb, 2005), and for tungsten it is 166 W/mK (CMW Elkon, 2005). With this in mind it is clear that with an increase in the wt% of copper the thermal conductivity will increase (see Figure 3.8), but the maximum service temperature will decrease. For ELKONITE® 50W3 the maximum service temperature is between 735 and 1135°C (CES, 2000). The maximum service temperature of copper and tungsten is 350-620 and 1098-1483 K respectively (CES,

2000). Thermal conductivity for the different WCu alloys varies from about 190 to 390 W/mK. These are values measured by the different manufacturers as in Appendix A.

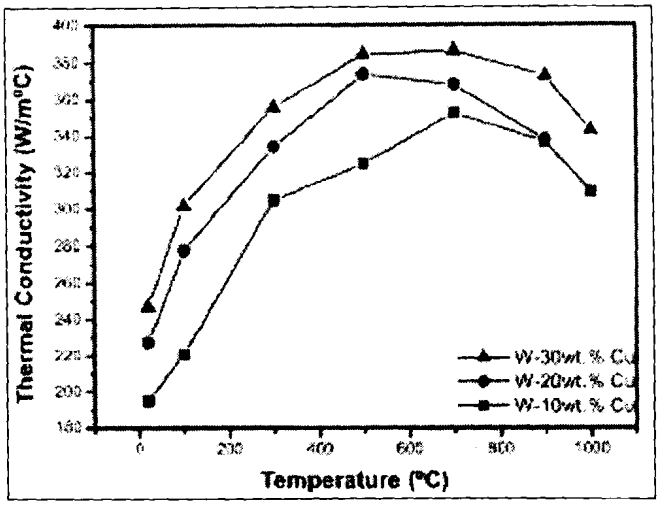

Figure 3.8 Temperature dependence of thermal conductivity of WCu (Kim *et al.* 2004).

Figure 3.9 is a plot of what happens to the thermal conductivity with an increase in temperature of some metals. It is clear that with an increase in temperature there is a decrease in thermal conductivity for both W and Cu. But with the combination of the two materials in WCu this is not the case. Figure 3.7 is a plot of the temperature dependence of thermal conductivity of WCu. It is clear that with an increase in temperature there is an increase in the thermal conductivity of the different alloys. This is the case up to a temperature in the region of 550-600°C. As the maximum operating temperature of the PBMM plant is 527.7°C, the decrease in thermal conductivity at higher temperatures does not affect the material selection for this specific study.

The thermal expansion of WCu also varies as the wt% of copper varies. Tungsten has a very low thermal expansion, 4.2-4.4μm /K, while that of copper is much higher, 16.9-18μm /K. Thus as the copper content increases so will the thermal expansion of the alloy. For the thermal expansion of WCu found in the literature study, see Appendix A-1.

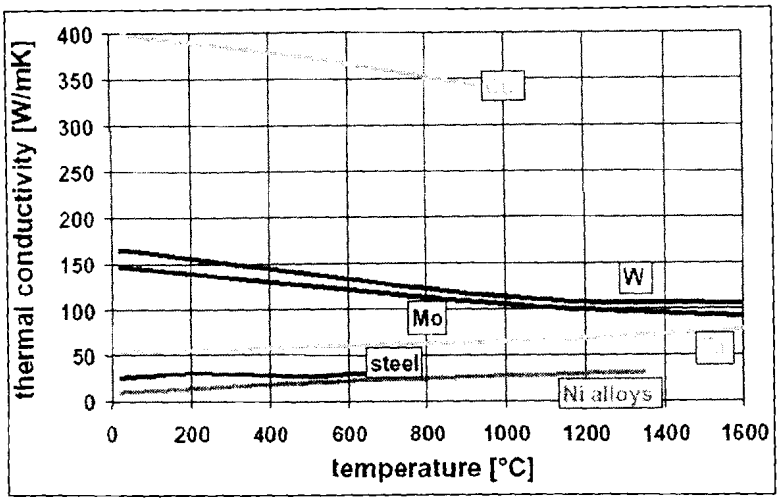

Figure 3.9 Temperature dependence of thermal conductivity of some metals (Smid & German, 2003).

At room temperature the composites behave in a brittle manner. Regardless of the hardness and brittle nature of this material, it could be machined using cemented carbide tools, (Machining Popular ELKONITE materials, 2005).
Material with a copper content of 5-45 wt% is commonly available at most manufacturers as listed in Appendix A-1. Material is available as sheets or could be ordered as finished parts, (Technical information CMW Inc, 2005) & (Barabash *et al.*, 2000:1248).

From the research on WCu it was found that CES only included one WCu in its database. Because WCu looks like a very good candidate material more WCu alloys were included in the list of candidate materials. The alloys included are listed in Table 3.4.

Table 3.4 Tungsten-copper alloys included as candidate materials.

Thermitech 75
ELKONITE® 1W3
ELKONITE® 3W3
ELKONITE® 3W53
ELKONITE® 5W3
ELKONITE® 2050C

3.4.1.3 Tungsten heavy metal alloys, (Lassner & Schubert, 1998).

The term tungsten heavy metal is used for a group of two-phase composites, based on W-Ni-Fe and W-Ni-Cu-(Fe). They are used wherever high density, excellent mechanical

properties, and good workability are required. Tungsten is the main component of these alloys (typically present in the range of 90 to 98 wt%) and the reason for their high density (between 17 and 18.5 g/cm^3). Nickel, iron, and copper serve as a binder matrix, which holds the brittle tungsten grains together and which makes the alloys ductile and easy to machine.

Heavy metals are produced by conventional powder metallurgy techniques. A flow chart of the fabrication process is shown in Figure 3.10. Elemental powders (W, Fe, Ni, and Cu) are blended in mixers or ball mills to the desired ratio, compacted to form a green body, and subsequently liquid-phase sintered. Assuming proper manufacturing conditions, they exhibit full or near-theoretical density in the as-sintered condition. Powder particle sizes are in the range of 2 to 6 μm. Both die pressing and isostatic pressing (dry- and wet-bag pressing) are in use. No lubricant is commonly added, since the green strength is high enough to handle the compacts. Powder injection molding is used for applications where net shaping is desired and large quantities of complex parts are produced. Sintering is commonly carried out in molybdenum-wire resistance-heated furnaces under hydrogen or nitrogen mixtures (dissociated ammonia) but can also be performed in vacuum units. The use of wet hydrogen has become industrial practice to suppress hydrogen embrittlement. The temperature/time program of the sintering cycle must be adjusted to the composition and size of the sintered parts. A cleaning step in hydrogen at 1000°C is commonly performed to render the outgassing of volatile compounds. High-purity powder grades must be used for sintering. Otherwise, blistering will occur on liquid-phase sintering, and interface precipitations will occur on cooling. Isothermal sintering is carried out above the eutectic temperature, typically between 1440 and 1500°C, but can be as high as 1600°C. The higher the tungsten content of the alloy, the higher the temperature. Tungsten-nickel-copper alloys are sintered at somewhat lower temperatures than tungsten-nickel-iron alloys. Sintering times are between 30 minutes and two hours. The solubility is highest in binary W-Ni alloys (up to 40 wt%; resulting in low ductility), but additions of Fe and Cu depress it to lower values (typically 20 to 25 wt% W), providing a tough and ductile binder matrix. Optimal mechanical properties require subsequent heat treatment of the alloys. Solution annealing at 900 to

1300°C and subsequent quenching to avoid impurity segregation and formation of intermetallic phases significantly improves ductility. Heavy metals can be cold-worked (swaged, rolled) to increase hardness and strengths at the expense of elongation and toughness. Aging at 500°C after 25% deformation (cold work) is a compromise to achieve both high ultimate tensile strengths and elongation. Conventional procedure is a double swaging-heat treatment cycle (deformation 25-30%). Heavy metals exhibit a ductile-to-brittle transition temperature. In comparison to pure tungsten it is, however, not a sharp transition but spreads over several hundred degrees. Although a considerable amount of densification already occurs during solid-state heating, isothermal liquid-phase sintering is a prerequisite to obtain near-theoretical density and a high degree of microstructural homogeneity. Rapid final densification occurs on formation of the liquid phase under the action of capillary forces. Particle rearrangements, solution/reprecipitation processes, and coalescence contribute to a higher packing density and a significant grain coarsening during sintering. The original tungsten powder grain size of 3-5 μm is transformed during sintering to rounded tungsten particles (spheroids) of at least 10 times the original grain diameter. Shape accommodation (formation of polyhedra with rounded corners) plays an important role in high tungsten alloys, where only a small quantity of liquid is available for achieving full density.

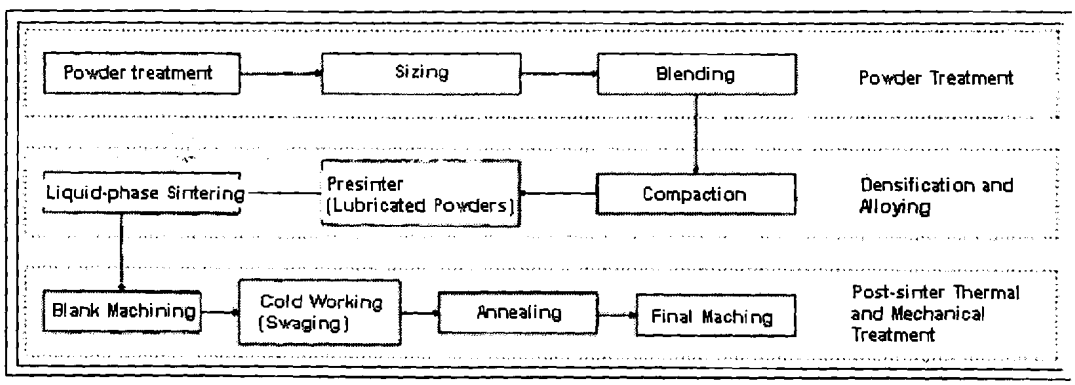

Figure 3.10 Manufacturing process of tungsten heavy metal alloys, (Lassner & Schubert, 1998).

The tungsten heavy metal alloys that are considered as material for the recuperator are Tungsten-2%Nickel-1%Iron alloy (ROSM WH9766F), Tungsten-3%Nickel-2%Iron alloy

(ROSM WH9560F), Tungsten-3.5%Nickel-1.5%Copper alloy (ROSM WH9570C), Tungsten-3.5%Nickel-1.5%Iron alloy (CMW 3950). Of these ROSM WH9570C is ranked as the best. Thermal conductivity for this material is 128 - 142 W/mK (CES, 2000). Thermal expansion for this material is also low, 4 - 4.9 μm/K (CES, 2000). It is one of the cheapest materials considered and can be machined.

3.4.2 Molybdenum and molybdenum alloys (H. Cross Co., 2005)

H. Cross Co. is the leading specialty metal rolling manufacturer of precision ribbons, sheets, foils and strips of molybdenum and molybdenum-base alloys. It also supplies wire, rod and a comprehensive line of custom and lamp industry products.

Molybdenum has a high melting temperature and it is impractical to transform it into ingot forms by conventional furnace melting techniques. Its manufacture by powder metallurgy consists of three distinct phases: the decomposition of the ore and its reduction to pure metal powder, the pressing of this powder into bars and the sintering of these bars into solid ingots and the swaging, rolling or drawing of these ingots into desired forms and sizes. Some products are fabricated from arc-cast ingots. Prefabricated or continuously compacted and sintered electrodes made from metal powder are arc-melted in a water-cooled copper mould. The process is usually carried out in a vacuum, although in some instances inert-atmosphere melting is employed.

After drawing or rolling operations have been completed, the material may be cleaned by exposure to elevated temperatures in a reducing atmosphere. Treating the surface chemically or electrolytically could also clean molybdenum. The material may be further reduced after processing by electrolytic etching.

3.4.2.1 TZM Alloys (titanium, zirconium, molybdenum)

Molybdenum's prime alloy is TZM. This alloy contains 99% Mo, 0.5% Ti and 0.08% Zr. TZM offers twice the strength of pure molybdenum at temperatures over 1300°C, see

Figure 3.11 for the ultimate tensile strength temperature dependence. The recrystallization temperature of TZM is approximately 250°C higher than molybdenum and it offers better weldability than pure molybdenum. The working temperature for TZM is above 600°C (Zinkle & Ghoniem), see Figure 3.12. TZM's finer grain structure and the formation of TiC and ZrC in the grain boundaries inhibit grain growth and the related failure of the base metal as a result of fracturing along grain boundaries. This characteristic also gives it better properties for welding. According to *Lienhard & Napolitano (1998)*, there is a drop in thermal conductivity form 120 to 100 W/mK if TZM is heated from 21 to 1090°C.

TZM generally costs around 25% more than pure molybdenum but in high heat and strength applications it can be well worth the cost differential.

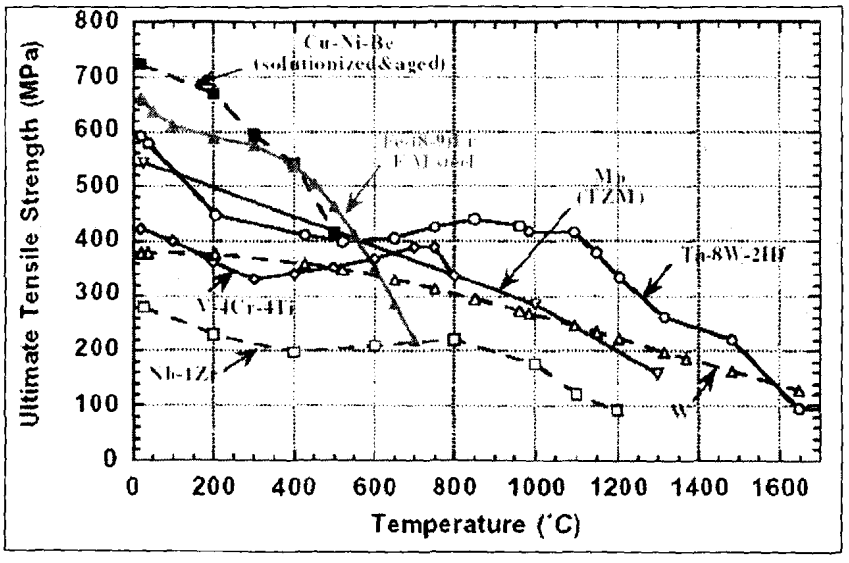

Figure 3.11 Comparison of the ultimate tensile strength of recrystallized refractory alloys, (Zinkle & Ghoniem).

TZM is generally available in sheet and foil in the same size ranges as pure molybdenum with the exception of very thin foil.

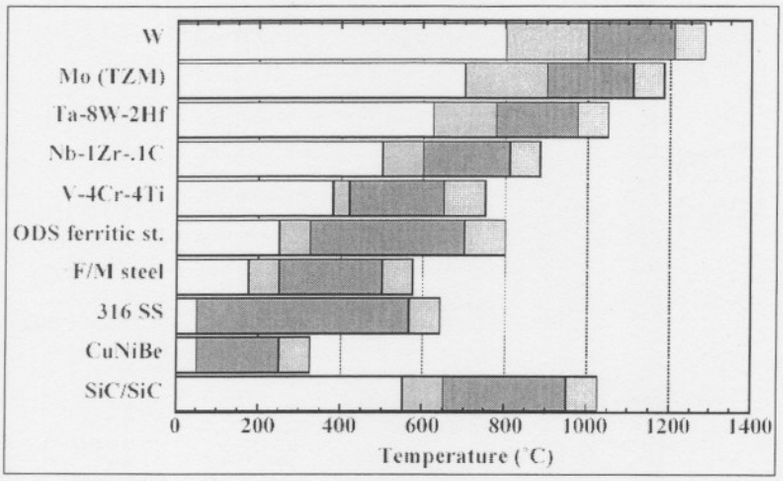

Figure 3.12 Operating temperature windows (based on radiation damage and thermal creep considerations) for refractory alloys. The light shaded bands on either side of the dark bands represent the uncertainties in the minimum and maximum temperature limit, (Zinkle & Ghoniem).

3.5 DECISION MATRIX

A decision matrix is used to identify the material that is the best choice for the application. In these methods, all the properties that are required to make a material suitable for the application are given a value of importance to get the right combination of properties.

3.5.1 Method used (Ashby, 1997)

In this stage of the material selection process only the candidate materials in Table 3.3 and Table 3.4 are considered. The decision matrix method that is used to select the best suited material is called the Weighted Property Index Method (WPIM).

3.5.2 Weighted Property Index Method (Ashby, 1997)

The WPIM is a method that ranks the materials in an order from the material with the most suitable collection of properties to the least suitable material. It is done by assigning a weight factor to each property. These weight factors are indications of the importance of a specific property. A drawback of this method is that it has to combine

different units. Properties are therefore normalized with the use of a scaling factor. The scaled value of a property, β, is given by:

$$\beta = \frac{Numerical\ \ value\ \ of\ \ property}{Largest\ \ value\ \ in\ \ the\ \ list}(100) \tag{3.13}$$

if the maximum of the property is required. In the case where the minimum value is the best for the application the scaled value of a property, β, is given by:

$$\beta = \frac{Lowest\ \ value\ \ in\ \ the\ \ list}{Numerical\ \ value\ \ of\ \ property}(100) \tag{3.14}$$

Table 3.5 is a list of the important properties of all the candidate materials.

Table 3.5 Important properties of the candidate materials.

Materials	Thermal Conductivity (W/mK)		Price (R/kg)		Hardness (MPa)		Elastic Limit (MPa)		Density (Mg/m^3)		Specific Heat (J/kgK)		Thermal Expansion (10^-6/K)	
Molybdenum Alloy 362 (Mo-0.5Ti alloy)	110	125	30.16	241.25	2500	3500	740	910	10.1	10.3	255	275	5.4	6.2
Molybdenum Alloy 363 (TZM Alloy)	129	147	35.18	251.31	2600	3600	770	950	10.05	10.25	255	275	4.7	5.5
Molybdenum Alloy 366 (Mo-30W alloy)	100	130	50.26	251.31	2500	3000	650	800	11.8	12	210	220	4	6
Molybdenum Titanium Alloy	110	147	36.75	306.20	2500	3600	740	950	10.05	10.3	255	275	4.7	6.2
Molybdenum Tungsten Alloy	100	130	61.24	306.20	2500	3000	650	800	11.8	12	210	220	4	6
Molybdenum, Commercial Purity	127	147	36.75	293.95	1500	6500	170	2000	10.1	10.3	255	275	4.8	5.5
Tungsten - ASTM Class 1 (90%W)	70	100	97.98	183.72	2400	3900	430	965	16.9	17.3	130	140	4.3	6.3
Tungsten - ASTM Class 4 (97%W)	100	126	97.98	183.72	2500	3500	435	760	18.25	18.85	130	140	4.2	5.2
Tungsten-10%Copper alloy, "Elkonite 50W3"	80	100	97.98	183.72	2500	3200	430	790	17.1	17.3	130	140	5.7	6.3
Thermitech 75	189		200		1720		620		14.7		201		10.2	
ELKONITE® 1W3	260		200		1200		434		12.5		160		11.7	
ELKONITE® 3W3	240		200		1600		517		13.93		160		9.7	
ELKONITE® 3W53	165		200		1600		620		13.82		160		9.8	
ELKONITE® 5W3	235		200		1720		586		14.18		160		9.4	
ELKONITE® 2050C	275		200		1200		434		12.02		160		12.2	

Table 3.6 is a list of the properties of importance for the recuperator. It also shows how the weight factor of each property is determined.

Table 3.6 Weight factors for the properties of the recuperator

Propertiy	Decision Number																				Total	Weight factor
	1	2	3	4	5	6	7	8	9	10	11	12	13	14	15	16	17	18	19	20	21		
Thermal conductivity	1	1	1	1	1	1																6	0.29
Elastic Limit	0						1	1	1	1	1											5	0.24
Price		0					0					0	1	1	1							3	0.14
Specific Heat			0					0				1				0	1	1				3	0.14
Thermal expansion				0					0				0			1			0	0		1	0.05
Hardness					0					0				0			0		1		1	2	0.10
Density						0					0				0			0		1	0	1	0.05

As seen in Table 3.6 each property is compared to one another to see which of the two is the most important. The most important property is credited with 1, and the other with 0. In the end a total is determined for each property, which is then divided by the decision number to calculate the weight factor.

In order to maximize the heat that is transferred from the hot fluid to the cold fluid, the material has to have a very high thermal conductivity. This is therefore the most important property. To withstand the difference in pressure between the primary and secondary sides, the material has to have a high strength. The elastic limit of the material is therefore considered the second most important property for a material to be used in the recuperator.

The cost of the material is like always an important property. As specific heat determines the time for the material to reach steady state, this is also very important. Because the performance of the recuperator is more important than the price of the material, specific heat is more important than price.

Hardness is important because it will determine whether the material can be machined or not.

As the difference between the two sides is relatively small, and thermal differences only occur at start-up, the thermal expansion is not as important as the other properties.

The recuperator will be installed and left in one place. Because of this, the weight alone is not that important. The specific heat of the material already makes provision for the recuperator to reach steady-state as soon as possible.

Table 3.7 gives all the weighted properties of the candidate materials. As seen in Table 3.7 the properties for the materials have a minimum and maximum value. For the WPIM only the maximum index where considered, as only one value was available for the ELKONITE® alloys.

Table 3.7 Weighted properties

Materials	Thermal Condutivity (W/mK)		Price (R/kg)		Hardness (MPa)		Elastic Limit (MPa)		Density (Mg/m^3)		Specific Heat (J/kgK)		Thermal Expansion (10^-6/K)		Total
Weight Factor of property	0.29	0.29	0.14	0.14	0.10	0.10	0.24	0.24	0.05	0.05	0.14	0.14	0.05	0.05	1.00
Molybdenum Alloy 362 (Mo-0.5Ti alloy)	11.60	24.66	14.00	10.66	4.80	8.57	23.06	10.92	3.76	3.83	7.14	7.13	3.70	4.19	52.57
Molybdenum Alloy 363 (TZM Alloy)	13.60	29.00	12.00	10.23	4.62	8.33	24.00	11.40	3.78	3.85	7.14	7.13	4.26	4.73	55.02
Molybdenum Alloy 366 (Mo-30W alloy)	10.55	25.65	8.40	10.23	4.80	10.00	20.26	9.60	3.22	3.29	8.67	8.91	5.00	4.33	52.31
Molybdenum Titanium Alloy	11.60	29.00	11.49	8.40	4.80	8.33	23.06	11.40	3.78	3.83	7.14	7.13	4.26	4.19	51.36
Molybdenum Tungsten Alloy	10.55	25.65	6.89	8.40	4.80	10.00	20.26	9.60	3.22	3.29	8.67	8.91	5.00	4.33	50.47
Molybdenum, Commercial Purity	13.39	29.00	11.49	8.75	8.00	4.62	5.30	24.00	3.76	3.83	7.14	7.13	4.17	4.73	69.20
Tungsten - ASTM Class 1 (90%W)	7.38	19.73	4.31	14.00	5.00	7.69	13.40	11.58	2.25	2.28	14.00	14.00	4.65	4.13	58.86
Tungsten - ASTM Class 4 (97%W)	10.55	24.86	4.31	14.00	4.80	8.57	13.56	9.12	2.08	2.10	14.00	14.00	4.76	5.00	59.31
Tungsten-10%Copper alloy, "Elkonite 50W3"	8.44	19.73	4.31	14.00	4.80	9.38	13.40	9.48	2.22	2.28	14.00	14.00	3.51	4.13	56.45
Thermitech 75	19.93		2.11		6.98		19.32		2.59		9.05		1.96		61.94
ELKONITE® 1W3	27.42		2.11		10.00		13.53		3.04		11.38		1.71		69.18
ELKONITE® 3W3	25.31		2.11		7.50		16.11		2.73		11.38		2.06		67.20
ELKONITE® 3W53	17.40		2.11		7.50		19.32		2.75		11.38		2.04		62.50
ELKONITE® 5W3	24.78		2.11		6.98		18.26		2.68		11.38		2.13		68.32
ELKONITE® 2050C	29.00		2.11		10.00		13.53		3.16		11.38		1.64		70.81

Table 3.8 provides all of the candidate materials in the order from highest total weighted properties to the lowest.

Table 3.8 Sorted candidate materials selected

Materials	Total
ELKONITE® 2050C	70.814
Molybdenum, Commercial Purity	69.199
ELKONITE® 1W3	69.181
ELKONITE® 5W3	68.317
ELKONITE® 3W3	67.199
ELKONITE® 3W53	62.501
Thermitech 75	61.944
Tungsten - ASTM Class 4 (97%W)	59.310
Tungsten - ASTM Class 1 (90%W)	58.862
Tungsten-10%Copper alloy, "Elkonite 50W3"	56.447
Molybdenum Alloy 363 (TZM Alloy)	55.017
Molybdenum Alloy 362 (Mo-0.5Ti alloy)	52.575
Molybdenum Alloy 366 (Mo-30W alloy)	52.310
Molybdenum Titanium Alloy	51.364
Molybdenum Tungsten Alloy	50.475

3.6 FINAL MATERIAL SELECTION

With the use of the WPIM the candidate materials were ranked according to the importance of the properties required. The material that was found to be the best solution is Elkonite® 2050C.

32wt% W- 68wt% Cu, ELKONITE® 2050C, is manufactured by the infiltration of a porous tungsten structure method. The composition of this alloy is 50 volume% tungsten and the balance is made up with the copper. This means that the tungsten structure gives the necessary high temperature strength, while the copper provides the high thermal conductivity.

Properties at room temperature, 25°C, for this alloy are as follows (CMW Catalog series 1200, 2004)

- Hardness - 70 Rockwell B
- Density - 12.02 g/cm^3
- Thermal conductivity - 275 W/mK
- Thermal expansion - 12.2 m x10^6/°C
- Ultimate tensile strength - 965 MPa (140,000 psi)

Another characteristic of W-32wt% Cu that makes it a good choice is the fact that at the inlet temperature of the recuperator, 95.3°C, the thermal conductivity is about 300 W/mK as seen in Figure 3.8. The thermal conductivity is increasing for the whole working temperature of the recuperator. At the outlet, the temperature is 527.7°C and the thermal conductivity is more than 380W/mK. This value is very close to that of high conductivity copper at this temperature, but the material still has the necessary strength properties.

Chapter 4

RECUPERATOR DESIGN

4.1 INTRODUCTION

The aim of this chapter is to give detail on the design of the recuperator. The chosen construction for the recuperator is that of a mini-channel heat exchanger. As a mini-channel heat exchanger can be seen as a plate-fin heat exchanger with very small channels, most of the theory will relate to that of a plate-fin recuperator. This major assumption has to be made in order to design a compact recuperator, according to Smith (1997).

The material selected for the recuperator is a Tungsten-copper alloy. The composition of this material is W-32wt% Cu. For more detail on the material selection process, see Chapter 3.

Commonly used methods used to design recuperators are the Log Mean Temperature Difference (LMTD) method and the Effectiveness-NTU (ε-NTU) method. The ε-NTU method will be discussed in more detail as it is the method that was used for this study.

4.1.1 Requirements for the chosen recuperator

According to the problem statement, the currently employed shell-and-tube recuperator of the PBMM must be replaced by a more effective recuperator. The requirements for this new recuperator are as follow:

- Must have an effectiveness of more than 90%.
- The ΔP must be very small, less than 5% of the inlet pressure at the specific side.
- Be as compact as possible.
- Must be able to handle the high temperatures of the cycle.
- Must not fail under the pressures in the recuperator, mechanical strength.

- Must not fail due to thermal shocks.
- Must not fail due to corrosion by the working fluid, nitrogen.

The desired effectiveness is selected as 95% and the ΔP as 3%.

Parameters used were as in the conceptual design of the PBMM (Hasse, 2002). Table 4.1 is a summary of the most important parameters.

Table 4.1 Operating parameters of the PBMM (Hasse, 2002)

Low Pressure side	
Mass flow rate	1.148 kg/s
Inlet Pressure	257.7 kPa
Inlet temperature	527.7 °C
High Pressure side	
Mass flow rate	1.086 kg/s
Inlet Pressure	805 kPa
Inlet temperature	95.3 °C

4.2 DESIGN OF THE RECUPERATOR FOR STEADY-STATE

As discussed it was decided to use a mini-channel construction for the recuperator for the PBMM as this construction is ideal for gases, as working fluids, and have very high efficiencies.

The first step in the design process of the recuperator is to select the surface geometry for the heat transfer surfaces. The flow configuration chosen is a counterflow configuration.

As stated previously in this chapter, a mini-channel heat exchanger can be seen as a plate-fin recuperator. It can be described as alternate layers of extended surfaces separated by flat plates (Smith, 1997). A complete block is usually of brazed construction, although diffusion bonding can be used if the material is suitable.

For the counterflow design the first step is to determining the heat exchange duty of one slice. The complete exchanger is then made up of an appropriate number of these slices, as seen in Figures 4.1a and 4.1b.

According to Smith (1997) flow friction and heat transfer correlations must be based on the cell geometries for full-height surfaces. A full-height surface is defined as the space between the two plates which separates the one fluid from the other. To determine the correct pressure loss, the loss for an individual flow channel must be determined.

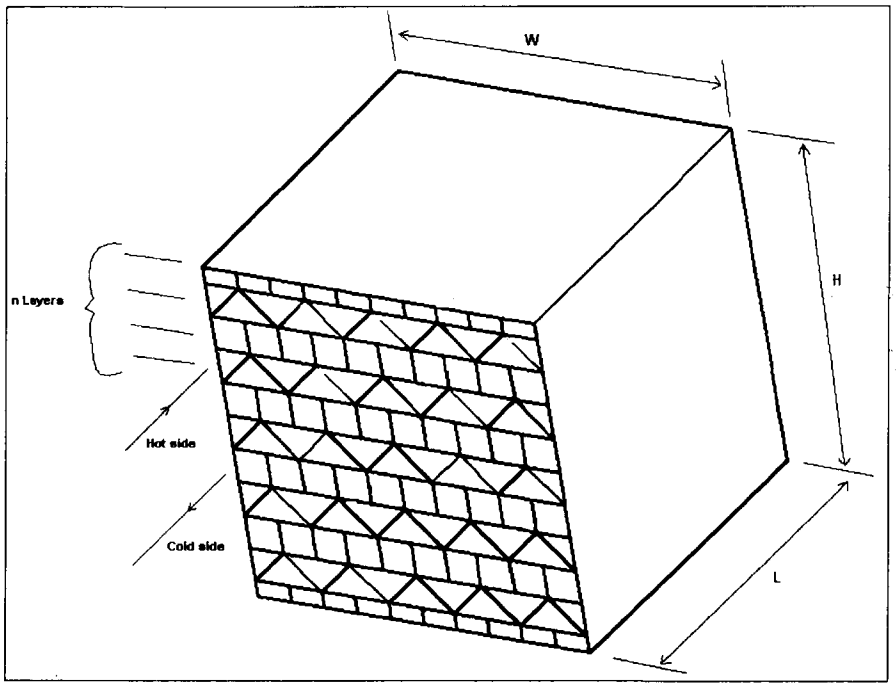

Figure 4.1a Counterflow plate-fin recuperator, modified from Smith (1997)

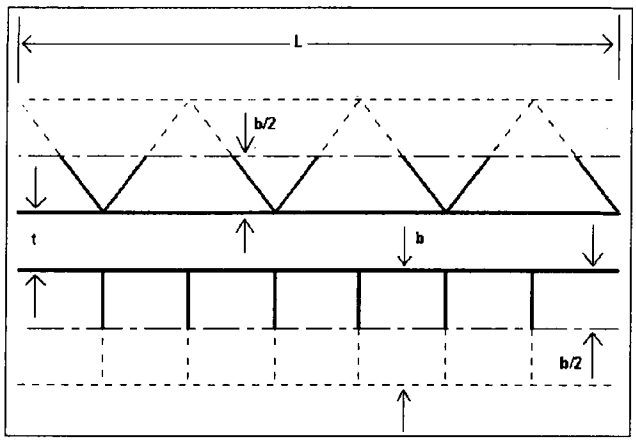

Figure 4.1b Design geometry for a counterflow plate-fin recuperator, modified from Smith (1997)

4.2.1 Rating of the recuperator

In a typical case the outlet temperature of the working fluid and the rate of heat transfer have to be determined for a recuperator. The effectiveness, ε, of a recuperator is given by:

$$\varepsilon = \frac{q}{q_{max}} \tag{4.1}$$

with q = the actual heat transfer and q_{max} = the maximum possible heat transfer.

To determine q_{max} the assumption is made that the recuperator has an infinite length, $L \rightarrow \infty$. The maximum possible heat transfer rate is the ideal rate that could be attained if one of the working fluids were to experience a maximum temperature difference in the recuperator (Kays & London, 1984).

$$q_{max} = C_{min} \Delta T_{max} \tag{4.2}$$

where $\Delta T_{max} = T_{h,i} - T_{c,i}$ (4.3)

$T_{h,i}$ = Inlet temperature of hot working fluid

$T_{c,i}$ = Inlet temperature of cold working fluid

$C_{min} = C_c$ if $C_c < C_h$

or $C_{min} = C_h$ if $C_c > C_h$

with $C_c = \dot{m}_c Cp_c$ en $C_h = \dot{m}_h Cp_h$ (4.4)

The ratio of the hot fluid capacity rate to the cold fluid capacity rate,

$$C_r = \frac{C_h}{C_c} \tag{4.5}$$

has a significant influence on the recuperator effectiveness.

The NTU (number of transfer units) indicates the relative heat transfer surface area. Mathematically, NTU is defined as:

$$NTU = \frac{UA}{C_{min}} \tag{4.6}$$

Kays & London (1984) have presented equations for NTU in terms of effectiveness and C_r, see Table 4.2.

To determine the outlet temperature for either the cold or the hot working fluid the following equation is used (Kays & London, 1984):

$$T_{h,e} = T_{h,i} - \frac{\varepsilon C_{\min}}{\dot{m}_h C_{p,h}} \left(T_{h,i} - T_{c,i}\right) \tag{4.7}$$

where the meaning of the subscripts are as follow:

e = Exit

h = Hot

c = Cold

i = Inlet

and $\dot{m}$ = Flow rate

Table 4.2 Recuperator Effectiveness Relations (Kays & London, 1984).

Counterflow:

$$\varepsilon = \frac{1 - e^{-NTU\left(1 - C_{min}/C_{max}\right)}}{1 - \left(C_{min}/C_{max}\right) e^{-NTU\left(1 - C_{min}/C_{max}\right)}} \quad (4.8)$$

Parallel flow:

$$\varepsilon = \frac{1 - e^{-NTU\left(1 + C_{min}/C_{max}\right)}}{1 - \left(C_{min}/C_{max}\right)} \quad (4.9)$$

Cross-flow
(Both fluids unmixed):

$$\varepsilon = 1 - e^{-NTU} \quad (4.10)$$

Cross-flow
(C_{min}=mixed , C_{max}=unmixed)

$$\varepsilon = 1 - e^{-\Gamma C_{max}/C_{min}} \quad (4.11)$$

with

$$\Gamma = 1 - e^{-NTU\left(C_{min}/C_{max}\right)} \quad (4.12)$$

Cross-flow
(C_{max}=mixed , C_{min}=unmixed)

$$\varepsilon = \frac{C_{max}}{C_{min}}\left(1 - e^{-\Gamma C_{min}/C_{max}}\right) \quad (4.13)$$

with

$$\Gamma = 1 - e^{-NTU} \quad (4.14)$$

Cross-flow
(Both fluids mixed):

$$\varepsilon = \frac{NTU}{\frac{NTU}{\left(1 - e^{-NTU}\right)} + \left(\frac{C_{min}}{C_{max}}\right)\frac{NTU}{\left(1 - e^{-NTU\left(\frac{C_{min}}{C_{max}}\right)}\right)} - 1} \quad (4.15)$$

Another very important, but often the most uncertain part of any recuperator analysis, is the determination of the overall heat transfer coefficient (UA). During normal operation, surfaces are often subject to fouling by fluid impurities, rust formation and other reactions between the fluid and the wall material. The subsequent deposition of a film or scale can greatly increase the resistance to heat transfer between the fluids.

The value of UA is calculated as follows (Incropera & De Witt, 2002):

$$\frac{1}{(UA)_c} = \frac{1}{(\eta_o hA)_c} + \frac{R''_{f,c}}{(\eta_o A)_c} \tag{4.16.1}$$

$$\frac{1}{(UA)_h} = \frac{1}{(\eta_o hA)_h} + \frac{R''_{f,h}}{(\eta_o A)_h} \tag{4.16.2}$$

with subscripts c and h referring to the cold and hot sides of the recuperator. All the areas are heat transfer areas.

The quantity η_o is termed the overall surface efficiency of a finned surface. It is defined such that, for the hot or cold surface without fouling, the heat transfer rate is:

$$q = \eta_o hA_t(T_b - T_\infty) \tag{4.17}$$

Where T_b is the base temperature, and

T_∞ is the temperature of the surrounding fluid.

R''_f is termed the fouling factor. Its value depends on the operating temperature, fluid velocity and length of service of the recuperator. For more on different types of fouling refer to Gupta (1986) and Somerscales (1997). But as clean and pure nitrogen is used for the cycle, negligible fouling is expected.

Heat transfer coefficients are calculated by using the Nusselt numbers, Nu. For laminar flow in square channels Nu is 2.98. By using the following equation for both the hot and cold sides, the heat transfer coefficients can be calculated:

$$h = Nu\frac{k}{D_h} \tag{4.18}$$

4.2.2 Geometry of the recuperator

It is the task of the designer to choose the dimensions to fit the need of the design. Figure 4.2a gives the basic geometric properties, while Figure 4.2b shows the geometry of a single cell which will be used in the design. The dimensions of the channels for the recuperator where chosen to be as follows:

- a = 0.001 m
- b = 0.001 m
- t_w = 0.001 m
- t_f = 0.0004 m

Some of the areas that have to be calculated in order to design this recuperator are as follows for the chosen configuration and dimensions:

Fin area:

$$A_f = n_w n_h 2bL \tag{4.19}$$

Total heat transfer area:

$$A_h = n_w n_h 2(a+b)L \tag{4.20}$$

Free-flow area:

$$A_{ff} = n_w n_h ab \tag{4.21}$$

It is also necessary to know the number of cells for the width and height of the recuperator. This is given by:

Number of cells high:

$$n_h = \frac{H}{2(b+t_w)} \tag{4.22}$$

Number of cells wide:

$$n_w = \frac{W}{a+t_f} \tag{4.23}$$

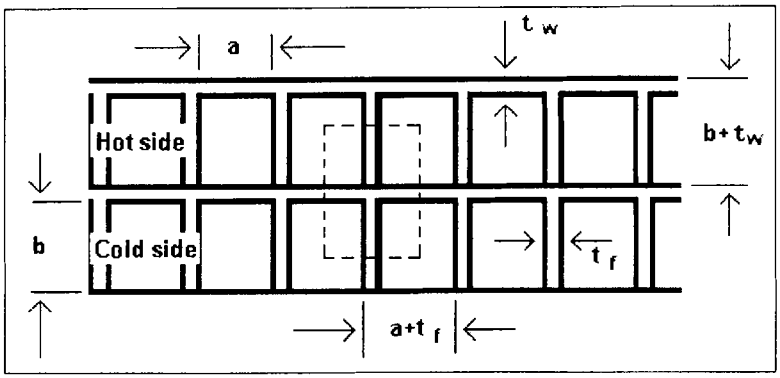

Figure 4.2a Basic geometry

For this geometry the hydraulic diameter is:

$$D_h = \frac{4A}{perimeter} = 2\frac{ab}{a+b} \tag{4.24}$$

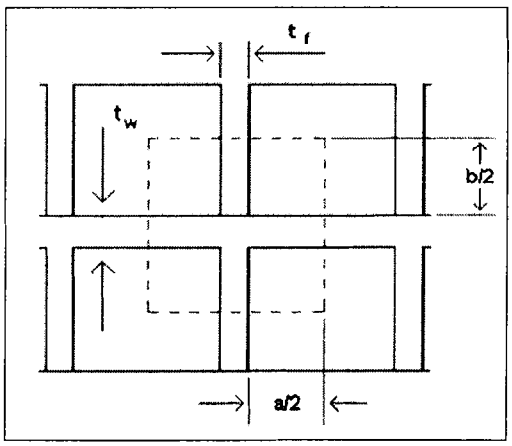

Figure 4.2b Enlargement of a single channel.

4.2.3 Fin performance

The assumption is made, that the mini-channel recuperator is made up of layers of flat-plates with extended surfaces. For this reason fin performance is very important.

Another way of defining η_o is:

$$\eta_o = 1 - \frac{A_f}{A_t}\left(1 - \eta_f\right) \tag{4.25}$$

where A_f is the entire fin surface area and η_f is the effectiveness of a single fin.

η_f can be calculate as follow:

$$\eta_f = \frac{Tanh(mL)}{mL} \tag{4.26}$$

with

$$m = \sqrt{\left(\frac{hP}{kA_c}\right)} \tag{4.27}$$

where P=Perimeter of the fin

A_c=Cross section area

4.2.4 Pressure drop

Pressure drop is energy that is lost. Pressure drop is a very important constraint for any recuperator design. As stated earlier, the desired ΔP is 3%. It is notable that the hot fluid side has a much higher ΔP% than the cold fluid side. Therefore if the hot side is within the prescribed limit, so will be the cold side. ΔP is calculated by the following equation:

$$\Delta P = \left(\frac{fL}{D_h} + \Sigma K\right)\frac{\left|\dot{m}\right|\dot{m}}{2\rho A_{ff}^{\ 2}} \tag{4.28}$$

with ΣK = 1.5 (0.5 for the inlet and 1 for the outlet for both the cold and hot sides).

4.3 DESIGN EVALUATION

For the evaluation of performance, the performance of the currently employed shell-and-tube recuperator was compared with that of the new compact recuperator. The influence of the new recuperator on the system was also investigated. As mentioned in Chapter 2, the paper by Gezelius (2004) is a good guideline for the evaluation of compact heat exchanger performance.

The design was evaluated with the use of a simulation of the heat exchanger. Design results were then compared with this simulation to determine the accuracy of the results. EES was used to do all calculations for the design of the new recuperator, while Flownex was used to validate the results that were generated by EES.

4.3.1 Design results

The design of the recuperator was done with the help of EES. For the complete EES-code that was used to design the recuperator see Appendix B-1.

According to Kays & London (1984), the variation in fluid properties in the flow direction of the heat exchanger is of more importance than the variation over the cross section of the flow channels. If the absolute temperature variation, from one end of the flow tube to the other, is less than 2:1 it is adequate to determine the fluid properties with the mean temperature (Tm). For greater temperature variations in the flow direction, it is probably better to consider the heat exchanger in separate sections, in each of which the temperature variation is not excessive. It was found that 20 increments were adequate as the difference in the results was less than 0.5% for more increments.

Appendix B-2 gives the results that were generated with the help of the EES-code. Table 4.3 is a summary of this and gives only the most important results of the EES-code.

The design requirements for the recuperator, as discussed previously in this chapter, were satisfied. Effectiveness for the recuperator is 95%, with a maximum percentage pressure drop on the hot side of 2.9%, while the cold side has a percentage pressure drop of 0.26%. The volume of the whole recuperator is only 0.3108m^3, with a footprint area of less than 0.4m^2 and with a surface-area density of 714.3m^2/m^3 this recuperator is classified as a compact heat exchanger (Incropera & De Witt, 2002).

Table 4.3 Results for EES-code

Properties		
Flowrate for hot side	1.148	kg/s
Inlet pressure (Hot side)	257.7	kPa
Outlet pressure (Hot side)	250.268	kPa
Epsilon_ph (Pressure drop, hot side)	2.884	%
Inlet temperature (Hot side)	527.7	°C
Outlet temperature (Hot side)	141.2	°C
Flowrate for cold side	1.084	kg/s
Inlet pressure (Cold side)	805	kPa
Outlet pressure (Cold side)	802.961	kPa
Epsilon_pc (Pressure drop, cold side)	0.2533	%
Inlet temperature (Cold side)	95.3	°C
Outlet temperature (Cold side)	505.3	°C
Epsilon (Effectiveness)	95.16	%
Height	0.8	m
Number of unit cells high	200	
Length	0.75	m
Width	0.518	m
Number of channels wide	370	
Mass	2404	kg
Volume	0.3108	m^3
Free-flow area	0.074	m^2
Alpha (Surface-area density)	714.3	m^2/m^3

4.3.2 Flownex model and results

Flownex was used to verify the results generated by EES. A model was used to simulate a compact heat exchanger. Figure 4.3 is an illustration of this model.

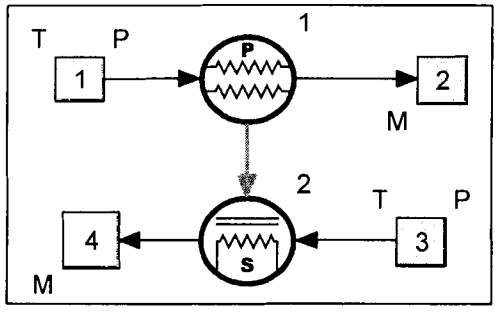

Figure 4.3 Illustration of the Flownex model.

Table 4.4 gives all the input values for the Flownex model. For the results of this simulation see Appendix B-3. Table 4.5 is a summary of the most important results of the Flownex simulation.

The effectiveness of the recuperator according to the Flownex simulation is 94.8%. As seen in Table 4.5 the outlet pressure at the primary and secondary sides are 250.44 kPa

and 802.98 kPa respectively. The temperatures are 141.8 °C and 505.4 °C respectively. This means that there is a maximum pressure drop of 2.8% at the primary side while for the secondary side the pressure drop is only 0.25%. As geometry for the Flownex model is required for the Flownex model, the same values that were calculated by the EES-code were used as an input for the Flownex model.

Table 4.4 Flownex input values

Identity	
Fluid	Nitrogen000_48_071200 (Const dens)
Element description	Recuperator
Heat exchanger type	Counter flow
Heat exchanger data	
Heat transfer area	222 m^2
Heat transfer area ratio	1
Fluid path length	0.75 m
Increments	20
Wall thickness	0.001 m
Material [User defined]	WCu
Mass	2404 kg
Flow data	
Primary side	
Inlet hydraulic diameter	0.001 m
Outlet hydraulic diameter	0.001 m
Inlet area	0.074 m^3
Outlet area	0.074 m^3
Laminar friction factor multiplier	1
Roughness	50 µm
Laminar Nussult number	2.98
Temperature at node 1	527.7 °C
Pressure at node 1	257.7 kPa
Flow rate at node 2	1.148 kg/s
Secondary side	
Inlet hydraulic diameter	0.001 m
Outlet hydraulic diameter	0.001 m
Inlet area	0.074 m^3
Outlet area	0.074 m^3
Laminar friction factor multiplier	1
Roughness	50 µm
Laminar Nussult number	2.98
Temperature at node 3	95.3 °C
Pressure at node 3	805 kPa
Flow rate at node 4	1.086 kg/s

Table 4.5 Results for Flownex simulation

Properties		
Flowrate for hot side	1.148	kg/s
Inlet pressure (Hot side)	257.7	kPa
Outlet pressure (Hot side)	250.44	kPa
Epsilon_ph (Pressure drop, hot side)	2.817	%
Inlet temperature (Hot side)	527.7	°C
Outlet temperature (Hot side)	141.8	°C
Flowrate for cold side	1.084	kg/s
Inlet pressure (Cold side)	805	kPa
Outlet pressure (Cold side)	802.983	kPa
Epsilon_pc (Pressure drop, cold side)	0.251	%
Inlet temperature (Cold side)	95.3	°C
Outlet temperature (Cold side)	505.4	°C
Epsilon (Effectivity)	94.84	%
Height	0.8	m
Number of unit cells high	200	
Length	0.75	m
Width	0.518	m
Number of channels wide	370	
Mass	2404	kg
Volume	0.3108	m^3
Free-flow area	0.074	m^2
Alpha (Surface-area density)	714.3	m^2/m^3

4.3.3 Comparison of the results

To compare the two sets of results, only the pressures and temperatures at the nodes on the different sides were considered. The percentage error between the two sets of results was calculated. Table 4.6, Figure 4.4 and Figure 4.5 are summaries of the results generated by the two methods and the percentage difference between them.

It was found that the maximum difference between the two sets of results is 0.76%. This is very small and thus it is clear that the two models match very closely. The difference in the effectiveness is calculated as 0.33%.

The results of the EES model can be taken as accurate, because it was verified with the Flownex model with an error of less than 1%.

Table 4.6 Comparison of the EES and Flownex data

Node	EES				Flownex				% error			
	Hot side		Cold side		Hot side		Cold side		Hot side		Cold side	
	P	T	P	T	P	T	P	T	P	T	P	T
	[kPa]	[°C]	[kPa]	[°C]	[kPa]	[°C]	[kPa]	[°C]	[kPa]	[°C]	[kPa]	[°C]
1	257.7	527.7	805	95.3	257.7	527.7	805	95.3	0	0	0	0
2	257.111	511.8	804.937	116.8	257.17	511.79	804.95	117.21	0.023	0.002	0.002	0.351
3	256.594	495.4	804.884	138.6	256.65	495.49	804.9	139.3	0.022	0.018	0.002	0.505
4	256.093	478.6	804.827	160.6	256.15	478.85	804.84	161.55	0.022	0.052	0.002	0.592
5	255.609	461.3	804.764	182.7	255.67	461.88	804.78	184.03	0.024	0.126	0.002	0.728
6	255.143	443.4	804.695	205	255.21	444.46	804.71	206.52	0.026	0.239	0.002	0.741
7	254.694	425.2	804.621	227.2	254.76	426.49	804.63	228.92	0.026	0.303	0.001	0.757
8	254.263	406.5	804.542	249.3	254.33	407.63	804.55	250.89	0.026	0.278	0.001	0.638
9	253.851	387.4	804.457	271.3	253.92	388.53	804.47	272.86	0.027	0.292	0.002	0.575
10	253.457	367.9	804.365	293	253.53	369.22	804.38	294.75	0.029	0.359	0.002	0.597
11	253.081	348	804.268	314.4	253.15	349.6	804.28	316.3	0.027	0.460	0.001	0.604
12	252.724	327.8	804.165	335.5	252.8	329.62	804.18	337.24	0.030	0.555	0.002	0.519
13	252.385	307.4	804.057	356.3	252.47	308.97	804.07	357.65	0.034	0.511	0.002	0.379
14	252.065	286.7	803.942	376.6	252.15	288.19	803.95	377.84	0.034	0.520	0.001	0.329
15	251.764	265.8	803.821	396.4	251.85	267.4	803.83	397.79	0.034	0.602	0.001	0.351
16	251.481	244.9	803.695	415.8	251.57	246.49	803.7	417.18	0.035	0.649	0.001	0.332
17	251.216	223.9	803.562	434.7	251.31	225.5	803.57	435.8	0.037	0.715	0.001	0.253
18	250.969	203	803.424	453.1	251.07	204.23	803.43	453.74	0.040	0.606	0.001	0.141
19	250.739	182.1	803.281	471	250.84	183.18	803.29	471.33	0.040	0.593	0.001	0.070
20	250.526	161.5	803.131	488.4	250.63	162.36	803.14	488.56	0.042	0.533	0.001	0.033
21	250.268	141.2	802.961	505.3	250.44	141.79	802.98	505.4	0.069	0.418	0.002	0.020

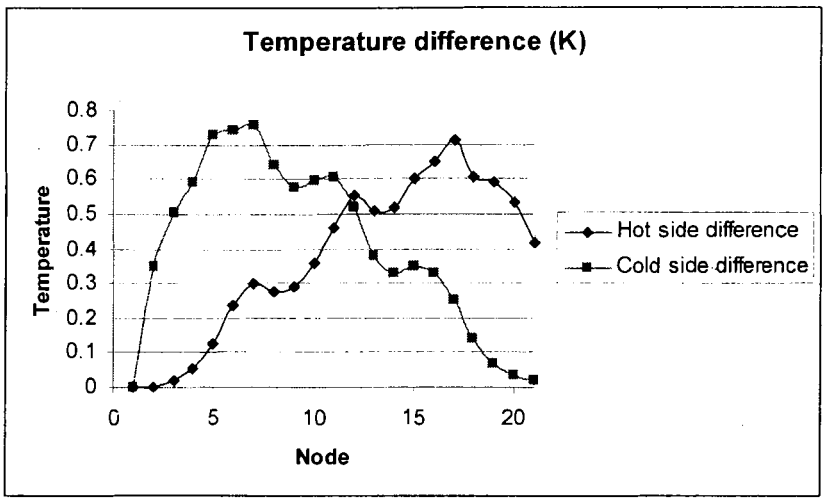

Figure 4.4 Temperature difference between EES and Flownex models.

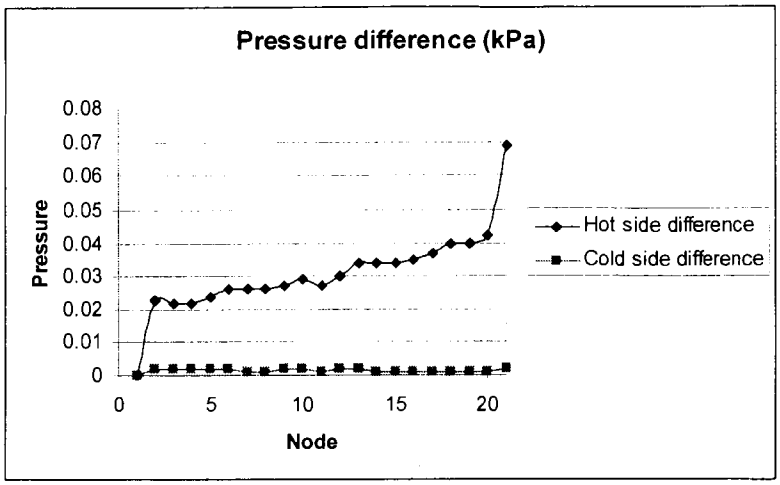

Figure 4.5 Pressure difference between EES and Flownex models.

4.4 DESIGNED RECUPERATOR

An outcome of this study is to design a more effective recuperator to replace the currently employed shell-and-tube recuperator of the PBMM. The material chosen for this recuperator is a Tungsten-copper alloy with 68 wt% W and 32 wt% Cu. It was decided to use a mini-channel heat exchanger with a counterflow configuration. This heat exchanger is made up of two types of plates that are stacked alternatively. The heat exchanger is then either diffusion bonded or brazed to join these plates.

The final geometry is as follows:

- Total length = 0.75 m
- Total width = 0.518 m
- Total height = 0.8 m
- Number of channels wide = 370
- Number of channels high = 200
- Plate thickness = 1 mm
- Fin thickness = 0.4 mm
- Channel height = 1 mm
- Channel width = 1 mm

For the performance of the chosen recuperator see Table 4.7.

Table 4.7 Recuperator performance

Property	Value
Heat transferred	479.528 kW
Heat transfer area density (α)	714.3 m^2/m^3
Mass	2404 kg
Outlet temperature (Cold side)	505.3 °C
Outlet temperature (Hot side)	141.2 °C
Pressure drop (Cold side)	0.2533 %
Pressure drop (Hot side)	2.884 %
Recuperator effectiveness	95.16 %
Volume	0.3108 m^3

Chapter 5

EVALUATION AND PERFORMANCE OF THE PROPOSED RECUPERATOR

5.1 PERFORMANCE EVALUATION

To evaluate the performance of the new recuperator it was compared with the currently employed shell-and-tube recuperator. The new recuperator is modified to have the same effectivity as the current shell-and-tube recuperator. The data of these two situations are then compared.

5.1.1 Shell-and-tube recuperator

Data of the currently employed recuperator for the PBMM is taken from the Flownex® simulation, M400_modified. Table 5.1 is a summary of its dimensions and properties. The performance properties are for the design specification. An advantage of this recuperator is its very low pressure drop for both the shell and the tube sides. In both cases it is lower than 0.5%. The total heat transferred is 440.72 kW with effectiveness of 87.7%.

5.1.2 Evaluation

With the help of EES the dimensions of the newly designed recuperator were changed, to design a recuperator with an effectiveness of 87%. This was done to make a direct comparison of the two recuperator types. Then a comparison was made between the new compact and the currently employed shell-and-tube recuperator. All the constant properties are eliminated from Tables 5.1-5.3 as it is the same for all three the recuperators. See Table 5.2 for the comparison between the 87% compact and shell-and-tube recuperators, and Table 5.3 for the comparison between the 95% compact and shell-and-tube recuperators.

Table 5.1 Shell-and-tube recuperator data

Properties		
Flowrate for hot side	1.148	kg/s
Inlet pressure (Hot side)	257.7	kPa
Outlet pressure (Hot side)	256.547	kPa
Epsilon_ph (Pressure drop, hot side)	0.447	%
Inlet temperature (Hot side)	527.7	°C
Outlet temperature (Hot side)	151.81	°C
Flowrate for cold side	1.084	kg/s
Inlet pressure (Cold side)	805	kPa
Outlet pressure (Cold side)	802.391	kPa
Epsilon_pc (Pressure drop, cold side)	0.324	%
Inlet temperature (Cold side)	95.3	°C
Outlet temperature (Cold side)	474.52	°C
Epsilon (Effectiveness)	87.7	%
Height (Shell diameter)	0.7	m
Length	6	m
Width (Shell diameter)	0.7	m
Mass	2391	kg
Footprint area	4.2	m^2
Volume	2.309	m^3
Alpha (Surface-area density)	111.74	m^2/m^3
Heat transferred	440.718	kW

Table 5.2 Comparison between the 87% compact and shell-and-tube recuperators

Properties	87% Compact	Shell-and-tube		Difference	%
Outlet pressure (Hot side)	250.428	256.547	kPa	6.119	2.385
Epsilon_ph (Pressure drop, hot side)	2.822	0.447	%	-2.374	530.703
Outlet temperature (Hot side)	176.11	151.81	°C	-24.3	16.007
Outlet pressure (Cold side)	803.14	802.391	kPa	-0.749	0.093
Epsilon_pc (Pressure drop, cold side)	0.231	0.324	%	0.093	28.708
Outlet temperature (Cold side)	471.1	474.52	°C	3.420	0.721
Epsilon (Effectiveness)	86.91	87.7	%	0.790	0.901
Height	0.64	0.7	m	0.060	8.571
Length	0.5	6	m	5.5	91.667
Width	0.434	0.7	m	0.266	38
Mass	1618	2391	kg	773	32.330
Foot print area	0.217	4.2	m^2	3.983	94.833
Volume	0.1389	2.309	m^3	2.170	93.984
Alpha (Surface-area density)	714.3	111.74	m^2/m^3	-602.563	539.271
Heat transferred	436.598	440.718	kW	4.120	0.935

Table 5.3 Comparison between the 95% compact and shell-and-tube recuperators

Properties	95% Compact	Shell-and-tube		Difference	%
Outlet pressure (Hot side)	250.268	256.547	kPa	6.279	2.448
Epsilon_ph (Pressure drop, hot side)	2.884	0.447	%	-2.437	544.585
Outlet temperature (Hot side)	141.2	151.81	°C	10.610	6.989
Outlet pressure (Cold side)	802.961	802.391	kPa	-0.57	0.071
Epsilon_pc (Pressure drop, cold side)	0.2533	0.324	%	0.071	21.845
Outlet temperature (Cold side)	505.3	474.52	°C	-30.780	6.487
Epsilon (Effectiveness)	95.16	87.7	%	-7.460	8.506
Height	0.8	0.7	m	-0.1	14.286
Length	0.75	6	m	5.25	87.5
Width	0.518	0.7	m	0.182	26
Mass	2404	2391	kg	-13	0.544
Foot print area	0.3885	4.2	m^2	3.812	90.75
Volume	0.3108	2.309	m^3	1.998	86.540
Alpha (Surface-area density)	714.3	111.74	m^2/m^3	-602.563	539.271
Heat transferred	479.528	440.718	kW	-38.810	8.806

5.1.2.1 Pressure drop

The pressure drop in both cases is much lower for the shell-and-tube recuperator than for the compact recuperators. In both cases, the compact recuperator hot side pressure drop is more than five times that of the shell-and-tube recuperator. For the cold side the compact recuperator has a pressure drop of 30% more than the shell-and-tube recuperator.

According to the design specification the recuperator must have a pressure drop of less than 5%. As the pressure drop for the 95% compact recuperator is only 2.9%, it is acceptable for the pressure drop to be higher than that of the shell-and-tube recuperator.

5.1.2.2 Outlet temperature

Outlet temperature is directly dependent on the effectivity of the recuperator. As the effectivity is nearly the same for the 87% compact and shell-and-tube recuperators, so are the outlet temperatures for both sides. In the case of the 95% compact and shell-and-tube recuperators, the outlet temperature for the 95% compact recuperator is about 8.5% higher.

5.1.2.3 Dimensions

As mentioned in Chapter 2, this is the category where the compact heat exchangers outperform the shell-and-tube heat exchangers.

In the case of the 87% compact and shell-and-tube recuperators, the 87% compact recuperator is much smaller. Its footprint area is only 5%, while the volume is only 6% of the shell-and-tube recuperator's volume.

The 95% compact recuperator's volume is nearly double that of the 87% compact recuperator. But in the case of the 95% compact and shell-and-tube recuperators, the 95% compact recuperator is much smaller. Its footprint area is only 10%, while the volume is only 13.5% that of the shell-and-tube recuperator.

Although the volume of the compact recuperators is less than that of the shell-and-tube recuperator, the weight of the 95% compact recuperator is 0.544% more than that of the shell-and-tube recuperator. This is because of the construction of a compact heat exchanger and because of the difference in the densities of the materials used. The density of the tungsten copper alloy is almost twice that of stainless steel AISI 304, which was used to build the shell-and-tube recuperator.

5.1.2.4 Heat transferred

As the primary function of a recuperator is to transfer heat, the effectiveness is measured by the amount of heat transferred from one fluid to the other.

The heat transferred for the 95% compact recuperator is 8.8% more than that of the shell-and-tube recuperator.

5.1.2.5 Response time

Another factor that is important in a recuperator is the response time, thus the time to steady state. To evaluate this, a Flownex simulation was done with a transient step that takes the recuperator from 25°C to the working temperatures. The time to steady state is then determined by taking the time where the outlet temperatures don't change anymore. This point is defined as that point where the temperature changes less that 0.001°C per time step.

For the 95% compact recuperator the response time is 1852 seconds, while it is 7494 seconds for the shell-and-tube recuperator. This means that the 95% compact recuperator reaches steady state in 24.7% of the time that the shell-and-tube recuperator does. See Figure 5.1 for a plot of the outlet temperatures with respect to time.

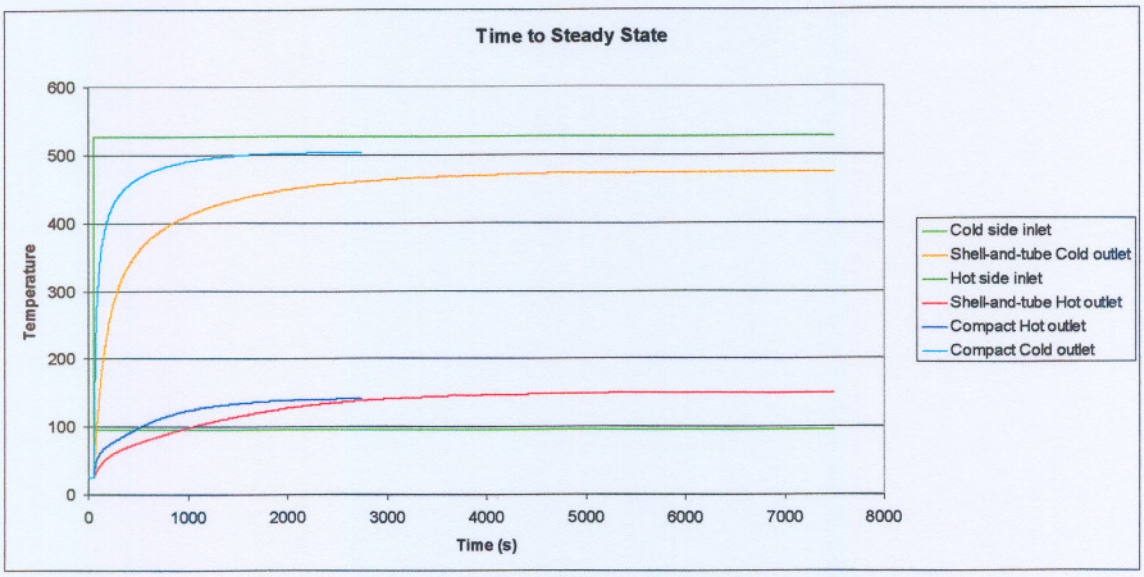

Figure 5.1 Temperatures vs. Time.

5.2 INFLUENCE ON THE PBMM CYCLE EFFICIENCY

The evaluation of the influence of the new recuperator on the PBMM is done by determining the influence of an increase in effectivity of the recuperator on the system effectivity. First an EES-code was generated, as explained by Rousseau & Greyvenstein (2002). This is used to see what will happen if the effectiveness of the recuperator is changed.

To determine the influence of the effectiveness of the recuperator on the PBMM cycle, the effectiveness of the recuperator is changed between 85 and 95%. It was decided on these values because the current recuperator has an effectiveness of 87% and the new

recuperator an effectiveness of 95%. Figure 5.2 illustrates how the cycle efficiency varies as the recuperator effectiveness is changed.

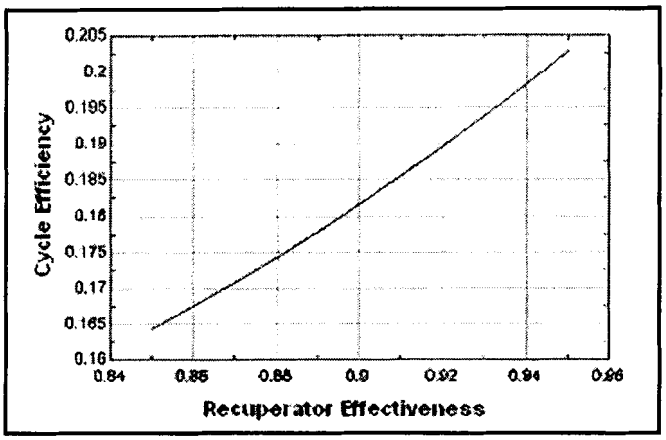

Figure 5.2 The impact of effectiveness of the recuperator on the PBMM cycle.

For the change from 87% to 95% for the recuperator effectivity there is a change of 3.19% in the cycle efficiency. This is an increase on the previous value of 18.67%.

To confirm this, the 95% compact recuperator is made part of the PBMM cycle simulation, M400_modified. This will take into account the thermo-hydraulic changes in the cycle. The cycle efficiency is determined before and after the compact recuperator is inserted. Before the compact recuperator was inserted the cycle efficiency was 19.4%. With the new compact recuperator the new cycle efficiency is 21.4%. This is an increase of 2%.

Chapter 6

CONCLUSION

6.1 CONCLUSIONS

This study included a material selection and optimization of a heat exchanger. For this material selection properties of materials at high temperature were taken in to account. The PBMM was used as constraining parameters for the material selection and design.

The material selected to be used in the high temperature recuperator, operating at temperatures between 90 and 530°C, was a tungsten-copper alloy with 68 wt% tungsten and 32 wt% copper. The main reason for selecting this material is because of its thermal conductivity at 530°C being nearly 390W/mK, which is nearly that of copper at room temperature.

It was found that a counterflow mini-channel (plate-fin) recuperator was the best construction to be used. For this mini-channel recuperator there are 370 channels in the width and 200 layers of cold and hot plates. The dimensions of each channel are 1x1mm.

The proposed recuperator was compared to the shell-and-tube recuperator currently employed in the PBMM cycle. It was found that it only occupies 10% of the foot print area and 13% of the volume of the shell-and-tube recuperator. Its effectiveness is 95%, which results in an increase 2% in the cycle effectiveness. The response time for the 95% compact recuperator is about 25% that of the shell-and-tube recuperator.

6.2 RECOMMENDATIONS FOR FURTHER STUDIES

For further studies there could be looked at a Marbond or printed circuit heat exchanger. The option of recuperators in an annular configuration with the turbines could also be investigated.

A method that may cause a decrease in the cost of the recuperator is the use of a bi-metal recuperator. The two materials which can be used are copper and WCu for the higher temperature regime.

The use of metallic foam as a fin material is another possibility which may increase the effectiveness of a recuperator as mentioned in the literature study.

Further investigation into silicon carbide as heat exchanger material is necessary. This material has very good properties as recuperator material, but was not selected due to the fact that the value of thermal conductivity is not clear. It also isn't clear whether silicon carbide is thermal shock resistant or not.

The possibility and effectiveness of coating, like diamond coatings, could be investigated.

REFERENCES

Ashby, M.F. 1997. Performance Indices, in Material Selection and Design, ASM Handbook (G.E. Dieter, a.o. eds.): *ASM International.* Vol. 20, p. 250-290. Materials park Ohio.

Ashby, M.F. 1999. Material Selection in Mechanical Design. 2nd ed. Oxford: Butterworth-Heinemann.

Babus'Haq, R.F., Akintunde, K., & Probert, S.D. 1995. Thermal performance of a pin-fin assembly. *Int. J. Heat and Fluid Flow*: Vol. 16, p50-55.

Barabash, V., Akiba, M., Cardella, A., Mazul, I., Odegard (Jr), B.C., Plöchl, L., Tivey, R.,& Vieider, G. 2000. Armor and heat sink materials joining technologies development for ITER plasma facing components: *Journal of Nuclear Materials,* Vol. 283-287, p1248-1252.

Boman, A., & Doty, D. 2002. Design and manufacture of ultra-low-mass, cryogenic heat exchangers. *Cryogenics*: Vol. 41, p797–803.

Boomsma, K., Poulikakos, D., & Zwick, F. 2003. Metal foams as compact high performance heat exchangers. *Mechanics of Materials*: Vol. 35, p1161–1176.

Cambridge Engineering Selector. CES Selector, Version 3.1: Granta Design Limited. 2000

CMW ELKON® Tungsten and Molybdenum Materials. http://www.cmwinc.com/TechInfo/wmo.htm. [Date of access 22 February 2005]

Esbeck D.W., Gates, S., & Schneider, P.H. 1997. Industrial Advanced Turbine Systems Program Overview. Solar Turbines Incorporated.

Gezelius, K. 2004. Design of Compact Intermediate Heat Exchangers for Gas Cooled Fast Reactors: Department of Nuclear Engineering; Massachusetts Institute of Technology.

Gupta, JP. 1986. Fundamentals of Heat Exchanger and Pressure Vessel Technology. New York: Hemisphere Publishing Corporation.

H. Cross Co. Molybdenum and Molybdenum alloys. http://www.hcrosscompany.com/refractory/molybdenum.htm. [Date of access 20 April 2005]

Hasse, G.W. 2002. Concept design report for the pebble modular reactor micro model (PBMM), M-Tech Industrial, report no.PBMM-0009.

Herman, C., & Kang, E. 2002. Heat transfer enhancement in a grooved channel with curved vanes. *International Journal of Heat and Mass Transfer*: Vol. 45, p3741–3757.

High-Density Tungsten Based Metals. Machining and Finishing. http://www.mi-techmetals.com/machin.htm. [Date of access 14 February 2005]

Hong, S.,& Kim, B. 2003. Fabrication of W-20 wt% Cu composite nanopowder and sintered alloy with high thermal conductivity: *Materials Letters*, Vol.57, p2761-2767.

Incropera, F.P., & De Witt, D.P. 2002. Fundamentals of Heat and Mass Transfer. 5th ed. New York, London, Sydney: John Wily & Sons Inc.

Kakac, S., Bergles, A.E., Mayinger, F. 1981. Heat Exchanger: Thermal-Hydraulic Fundamentals and design. Washington, New York, London: Hemisphere Publishing Corporation.

Kays, W.M., & London, A.L. 1984. Compact heat exchangers. United States of America: McGrew-Hill Inc.

Kim, D.G., Kim, G.S., Oh, S.T.,& Kim, Y.D. 2004. The initial stage of sintering for the W–Cu nanocomposite powder prepared from W–CuO mixture: *Materials Letters*, Vol. 58, p578– 581.

Kim, J.C.,& Moon, I.H. 1998. Sintering of nanostructured W-Cu alloys prepared by mechanical alloying: *Nanostructured Materials*, Vol. 10, No. 2, p283-290.

Kim, Y.D., Oh, N.L., Oh, S.T.,& Moon, I.H. 2001. Thermal conductivity of W–Cu composites at various temperatures: *Materials Letters*, Vol. 51, p420–424.

Lassner, E.,& Schubert, W.D. 1998. Tungsten. Properties, Chemistry, Technology of the element, Alloys and Chemical compounds. Chapter 6: New York, Boston, Dordrecht, London, Moscow: Kluwer Academic/ Plenum Publishers.

Li, Y., Qu, X., Zheng, Z., Lei, C., Zou, Z.,& Yu, S. 2003. Properties of W–Cu composite powder produced by a thermo-mechanical method: *International Journal of Refractory Metals & Hard Materials,* Vol. 21, p259–264.

Lienhard, J.H.,& Napolitano, D.S. 1998. Yield limits of plates at extremely high heat flux. Massachusetts institute of Technology Cambridge: *Journal of Heat Transfer*, Vol.120.

Luzzatto, C., Morgana, A., Chaudourne, S., O'Doherty, T., & Sorbie, G. 1997. A new concept composite heat exchanger to be applied in high-temperature industrial processes. *Applied Thermal Engineering*: Vol. 17, p789-797.

Machining Popular ELKONITE® Materials. http://www.cmwinc.com/TechInfo/elkmach.htm. [Date of access 28 February 2005]

Manglik, R.M., & Bergles, A.E. 1995. Heat transfer and pressure drop correlations for the rectangular offset strip fin compact heat exchanger. *Experimental Thermal and Fluid Science*: Vol. 10, p171-180.

Manglik, R.M., Zhang, J., & Muley, A. 2005. Low Reynolds number forced convection in three-dimensional wavy-plate-fin compact channels: fin density effects. *International Journal of Heat and Mass Transfer*: Vol. 48, p1439–1449.

Matweb:AISI Type 347 Stainless Steel, annealed, bar. http://www.matweb.com/search/SpecificMaterialprint.asp. [Date of access 20 April 2005]

Matweb: Oxygen-free high conductivity Copper, Soft, UNS C10200. http://www.matweb.com/search/SpecificMaterial.asp?bassnum=MC102A. [Date of access 30 March 2005]

Maziasz, P.J., Pint, B.A., Swindeman, R.W., More, K.L., Shingledecker, J.P., & Evans, N.D. 2003. Advanced Alloys for High-Temperature Recuperators. Metals and Ceramics Division, Oak Ridge National Laboratory, Oak Ridge.

McDonald, C.F. 2003. Recuperator considerations for future higher efficiency microturbines. *Applied Thermal Engineering*: Vol. 23, p1463–1487.

Minhas, H., & Lock, G.S.H. 1996. Estimating the influence of Prandtl number on heat transfer. *Heat and Mass Transfer*: Vol. 23, p1011-1017.

Murray, R.L. 2000. Nuclear Energy: An Introduction to the Concepts, Systems and Applications of Nuclear Processes. 5th ed. Raleigh, North Carolina, USA: Butterworth-Heinemann.

Natesan, K., Purohit, A., Tam, S.W. 2003. Materials Behaviour in HTGR Environments. 20555-0001. Washington: U.S. Nuclear Regulatory Commission Office of Nuclear Regulatory Research.

O'Doherty, T., Jolly, A.J., & Bates, C.J. 2001. Optimization of heat transfer enhancement devices in a bayonet tube heat exchanger. *Applied Thermal Engineering*: Vol. 21, p19-36.

PBMR: HOW THE PEBBLE BED MODULAR REACTOR WORKS. www.PBMR.co.za. [Date of access 7 April 2004]

Properties of CMW metals, metal alloys and contact materials. Catalog series 1200: Contacts, Metals & Welding, Inc. 2004

Rousseau, P.G., & Greyvenstein, G.P. 2002. Conceptual Thermo-Hydraulic Design of the PBMR Micro Model, M-Tech Industrial, report no.PBMM-0001.

Sahin, A.Z. 1997. Thermodynamic design optimization of a heat recuperator. *Heat and Mass Transfer*: Vol. 24, p1029-1038.

Schleicher, R., Raffray, A.R. & Wong, C.P. 2000. An assessment of the Brayton cycle for high performance power plants: *Fusion Technology.*

Seong, B.G., Kim, K.Y., & Hwang, S.Y. 2000. High-temperature corrosion of recuperators used in steel mills. *Surface and Coatings Technology.* No. 126, p 256-265

Smid, I.,& German, R. 2003. Sintering and Shaping of Refractory Metals – CISP, Penn State; September 17 @ Sintering '03

Smith, E.M. 1997. Thermal Design of Heat Exchangers. A Numerical Approach. Chichester: John Wiley & Sons.

Smith, E.H. 2000. Mechanical Engineer's Reference Book. Oxford. Butterworth-Heinemann. Chapter 12, 12/3.

Somerscales, E.F.C. 1997. Fundamentals of Corrosion fouling. Department of Mechanical Engineering. Rensselaer Polytechnic Institute, Troy, New York: Experimental Thermal and Fluid Science, Vol. 14, p335-355.

Stainless Steel 347. http://www.principalmetals.com/properties/result.asp?Family=Stainless+Steel&MetalName=347. [Date of access 20 April 2005]

Tadrist, L., Miscevic, M., Rahli, O., & Topin, F. 2004. About the use of fibrous materials in compact heat exchangers. *Experimental Thermal and Fluid Science*: Vol. 28, p193–199.

Technical information CMW INC. The torch brazing of ELKONITE®S TO CMW® COPPER-BASE ALLOYS. http://www.cmwinc.com/TechInfo/elkbraze.htm. [Date of access 28 February 2005]

The Encyclopaedia of Alternative Energy and Sustainable living. www.daviddarling.info/encyclopedia. [Date of access 20 May 2005]

Thonon, B., & Breuil, E. 2000. Compact heat exchangers technologies for the HTRs. IAEA-TECDOC. Vol. 1238, p149-160.

Traverso, A., & Massardo, A.F. 2005. Optimal design of compact recuperators for microturbine application. *Applied Thermal Engineering*. Article in press.

Wang, J., Hirs, G.G., & Rollmann, P. 1999.The performance of a new gas to gas heat exchanger with strip fin. *Energy Conversion & Management*: Vol. 40, p1743-1751.

Whyatt, G.A. 2003. Micro-Channel Recuperator and Mixer for FASTER (Feasibility of Acceptable Start Time Experimental Reactor) Autothermal Reformer. Pacific Northwest National Laboratory. US Department of Energy.

Yan, X., Takizuka, T., Takada, S., Kunitomi, K., Minatsuki, I., & Mizokami, Y. 2003. Cost and performance design approach for GTHTR300 power conversion system. *Nuclear Engineering and Design*: Vol. 226, p351–373.

Zhou, Z.J.,& Kwon, Y.S. 2005. Fabrication of W–Cu composite by resistance sintering under ultra-high pressure: *Journal of Materials Processing Technology*, Still in press.

Zhu, J., & Zhang, W. 2004. Optimization design of plate heat exchangers (PHE) for geothermal district heating systems. *Geothermics*: Vol. 33, p337–347.

Zinkle, S.J.,& Ghoniem, N.M. 1999. Operating temperature windows for fusion reactor structural materials: Los Angeles, CA 90095, USA

Appendix A

TUNGSTEN COPPER ALLOYS

Appendix A will be giving more detail on Tungsten Copper Alloys.

CONTENTS

A-1 Common Tungsten Copper Alloys with their Manufacturers and Thermal properties.

Alloy	Wt %		Company	Thermal conductivity W/mK	Thermal expansion µm /K	Reference
	W	Cu				
Copper Infiltrated Tungsten	89.1	10.9	ATI Wah Chang	194	6.6	http://www.alleghenytechnologies.com [11]
WCu10	90	10	MarkeTech Internasional Inc	170-180	6.5	http://www.mkt-intl.com [12]
WCu15	85	15	MarkeTech Internasional Inc	190-200	7	http://www.mkt-intl.com [12]
WCu20	80	20	MarkeTech Internasional Inc	200-220	8.3	http://www.mkt-intl.com [12]
WCu25	75	25	MarkeTech Internasional Inc	220-250	9	http://www.mkt-intl.com [12]
Elkanite 20W3	75	25	Mallory Alloys Group	139	9.82	http://www.mallory.com [3]
NS-EMC10	90	10	Nippon Tungsten	205	6.8	http://www.nittan.co.jp [4]
THERMKON® 62	90	10	CMW Inc.	150-170	5.7-6.5	http://www.cmwinc.com [5]
THERMKON® 68	85	15	CMW Inc.	164-188	6.3-7.1	http://www.cmwinc.com [5]
THERMKON® 76	80	20	CMW Inc.	180-210	7.2-8	http://www.cmwinc.com [5]
THERMKON® 83	75	25	CMW Inc.	200-240	8.1-8.9	http://www.cmwinc.com [5]
WCu 70/30	70	30	H.C Starck	>150	9.5	http://www.hcstarck.de [6]
WCu 80/20	80	20	H.C Starck	>140	9.5	http://www.hcstarck.de [6]
WCu 85/15	85	25	H.C Starck	>162	8	http://www.hcstarck.de [6]
WCu 90/10	90	10	H.C Starck	>160	6.7	http://www.hcstarck.de [7]
W-10Cu	90	10	Materials Co.,ltd.	191	6.3	http://www.refractorymetal.net [8]
W-15Cu	85	15	Materials Co.,ltd.	198	7.1	http://www.refractorymetal.net [8]
W-20Cu	80	20	Materials Co.,ltd.	221	7.6	http://www.refractorymetal.net [8]
W-25Cu	75	25	Materials Co.,ltd.	235	8.5	http://www.refractorymetal.net [8]
W-30Cu	70	30	Materials Co.,ltd.	247	9	http://www.refractorymetal.net [8]
Thermitech 75	75	25	Mi-Tech Metals Inc.	189	10.22	http://www.mi-techmetals.com [9]
Thermitech 80	80	20	Mi-Tech Metals Inc.	182	9.2	http://www.mi-techmetals.com [9]
Thermitech 85	85	15	Mi-Tech Metals Inc.	175	7.97	http://www.mi-techmetals.com [9]
Thermitech 90	90	10	Mi-Tech Metals Inc.	147	6.49	http://www.mi-techmetals.com [9]
AWC 7525	75	25	AMETEK	231	9.55	http://www.ametekmetals.com [10]
AWC 8020	80	20	AMETEK	220	8.6	http://www.ametekmetals.com [10]
AWC 8515	85	15	AMETEK	208	7.65	http://www.ametekmetals.com [10]
AWC 8812	88	12	AMETEK	203	7	http://www.ametekmetals.com [10]
AWC 9010	90	10	AMETEK	197	6.7	http://www.ametekmetals.com [10]
W 60/Cu40	60	40		228	11.7	Goodfellow - Material Information [11]
Copelmet® W 72/Cu28	72	28		198	10.5	Goodfellow - Material Information [11]
ELKONITE® 1W3	55	45		150		http://www.matweb.com [12]
ELKONITE® 3W3	68	32		160		http://www.matweb.com [13]
ELKONITE® 5W3	70	30		160		http://www.matweb.com [14]
ELKONITE® 1W3	55	45	CMW Inc.	260	11.7	http://www.cmwinc.com [15]
ELKONITE® 3W3	68	32	CMW Inc.	240	9.7	http://www.cmwinc.com [15]
ELKONITE® 53W3	68	32	CMW Inc.	165	9.8	http://www.cmwinc.com [15]

A-1 Table A-1 (Continued)

Alloy	Wt %		Compony	Thermal conductivity W/mK	Thermal expansion µm /K	Reference
	W	Cu				
ELKONITE® 5W3	70	30	CMW Inc.	235	9.4	http://www.cmwinc.com [15]
ELKONITE® 10W3	75	25	CMW Inc.	220	8.5	http://www.cmwinc.com [15]
ELKONITE® 10W53	75	25	CMW Inc.	160	8.6	http://www.cmwinc.com [15]
ELKONITE® 30W3	80	20	CMW Inc.	195	7.6	http://www.cmwinc.com [15]
ELKONITE® 40W3	87	13	CMW Inc.	170	6.4	http://www.cmwinc.com [15]
ELKONITE® 50W3	90	10	CMW Inc.	160	6.1	http://www.cmwinc.com [15]
ELKONITE® 2050C	50	50	CMW Inc.	275	12.2	http://www.cmwinc.com [15]

A-2 References

[1] Powder Metals Data Sheets. http://www.alleghenytechnologies.com/WahChang/pages/products/data/powders/copptung.htm. [Date of access 22 February 2005].

[2] Tungsten-Copper Alloys. http://www.mkt-intl.com/tungsten/wcu.html. [Date of access 7 February 2005]

[3] Elkanite 20W3 Datasheet. http://www.mallory.com/data/html/1300107.htm. [Date of access 22 February 2005]

[4] Nippon Tungsten advances W-Cu composites. http://www.nittan.co.jp/english/news.htm. [Date of access 2 March 2005]

[5] THERMKON® Materials by CMW® Inc. http://www.cmwinc.com/TechInfo/tkeng.htm. [Date of access 22 February 2005]

[6] Tungsten copper composite materials. http://www.hcstarck.de/index.php?page_id=322. [Date of access 28 February 2005]

[7] Tungsten Copper. http://www.refractorymetal.net/eng/Tungsten-copper/. [Date of access 22 February 2005]

[8] Thermitech. http://www.mi-techmetals.com/thermat.htm. [Date of access 14 February 2005]

[9] Tungsten-Copper Metal Matrix Composites (AWC Series). http://www.ametekmetals.com/matrix-AWC.asp. [Date of access 22 February 2005]

[10] Tungsten/Copper W 60/Cu40. http://www.goodfellow.com/csp/active/gfMaterialInfo.csp?text=*T&MATID=W18&material=1. [Date of access 22 February 2005]

[11] Tungsten/Copper W 72/Cu28. http://www.goodfellow.com/csp/active/gfMaterialInfo.csp?text=*T&MATID=W18&material=1. [Date of access 22 February 2005]

[12] CMW ELKONITE® 1W3 (Copper Tungsten) RWMA Class 10. http://www.matweb.com/search/SpecificMaterial.asp. [Date of access 28 February 2005}

[13] CMW ELKONITE® 3W3 (Tungsten Copper material) ASTM B702. http://www.matweb.com/search/SpecificMaterial.asp. [Date of access 28 February 2005}

[14] CMW ELKONITE® 5W3 (Tungsten Copper material) ASTM B702, Class C, infiltrated. http://www.matweb.com/search/SpecificMaterial.asp. [Date of access 28 February 2005}

[15] Tungsten-Copper Elkonite® Materials. http://www.cmwinc.com/TechInfo/cuwelk.htm. [Date of access 22 February 2005]

Appendix B

HEAT EXCHANGER DESIGN

Appendix B will be giving more detail on the design of the mini-channel heat exchanger. The results of EES and Flownex will be compared to verify the results.

CONTENTS

B-1 EES SIMULATION

```
"Funksies"
"NTU"
Function NTU(C_r,epsilon)
   If (C_r<1) then
NTU=(1/(C_r-1)*ln((epsilon-1)/(epsilon*C_r-1)))
else
   if (C_r=1) then
NTU=epsilon/(1-epsilon)
else
   if (C_r=0) then
NTU=-LN(1-epsilon)
endif
endif
endif
end

"Nu-verhit"
Function Nu_verhit(Re,Pr)
   If (Re<2000) then
Nu_verhit=2.98
else
   if (2000<=Re) and (Re<=10000) then
Re_1=2000
Re_2=10000
Nu_1=2.98
Nu_2=0.023*10e4^0.8*Pr^0.4
DELTAx=log10(Re_2)-log10(Re_1)
DELTAy=log10(Nu_2)-log10(Nu_1)
m=DELTAy/DELTAx
c=log10(Nu_1)-m*log10(Re_1)
Nu_verhit=10^(m*log10(Re)+c)
else
   if (10000<=Re) then
Nu_verhit=0.023*Re^0.8*Pr^0.4
endif
endif
endif
end

"Nu-verkoel"
Function Nu_verkoel(Re,Pr)
   If (Re<2000) then
Nu_verkoel=2.98
else
   if (2000<=Re) and (Re<=10000) then
Re_1=2000
Re_2=10000
Nu_1=2.98
Nu_2=0.023*10e4^0.8*Pr^0.3
DELTAx=log10(Re_2)-log10(Re_1)
DELTAy=log10(Nu_2)-log10(Nu_1)
m=DELTAy/DELTAx
c=log10(Nu_1)-m*log10(Re_1)
```

```
Nu_verkoel=10^(m*log10(Re)+c)
else
    if (10000<=Re) then
Nu_verkoel=0.023*Re^0.8*Pr^0.3
endif
endif
endif
end

"Thermal conductivity of WCu"
Function k(T)
    K=224.215001 + 1.13349536*T - 0.00499440337*T^2 + 0.0000145760248*T^3 -
2.38575590E-08*T^4 + 1.95516530E-11*T^5 - 6.28842581E-15*T^6
end


"Algemeen"
"Konstantes"
    R_fh=0
    R_fc=0
    j=19

"geometrie"
    t_f=0.0004
    t_w=0.001
    a=0.001
    b=0.001
    L_totaal=1
        L=L_totaal/(j+1)
    n_h=220
    n_w=440
    n_h=H/(2*(b+t_w))
    n_w=(W/(a+t_f))

    "Area's"
        A_h=n_w*n_h*2*(a+b)*L
        A_ff=n_w*n_h*a*b
        A_f=2*n_w*n_h*(b)*L

    "Hidroliese diameter"
        D_h=2*((a*b)/(a+b))

"Given"
    T_hi[0]=527.7
    P_hi[0]=257.7e3
    m_dot_h=1.148
    T_ce[j]=95.3
    P_ce[j]=805e3
    m_dot_c=1.086

"Volume"
    Vol=L_totaal*H*W
    alpha=(A_h_tot)/Vol
    A_h_tot=A_h*(j+1)
```

```
"For flownex"
   Mass=rho_m*(H*W-A_ff)*L_totaal
   rho_m=14180

"Aannames"
   T_bar=(T_hi[0]+T_ce[j])/2

"Calculations"
   C_min[0]=MIN(C_h[0],C_c[0])
   C_max[0]=Max(C_h[0],C_c[0])
duplicate i=1,j-1
   C_min[i]=MIN(C_h[i],C_c[i])
   C_max[i]=Max(C_h[i],C_c[i])
end
   C_min[j]=MIN(C_h[0],C_c[0])
   C_max[j]=Max(C_h[0],C_c[0])


"Hot side"
"Properties"
   CP_h[0]=CP(Nitrogen,T=T_bar_h[0],P=P_bar_h[0])
   k_h[0]=CONDUCTIVITY(N2,T=T_bar_h[0])
   Pr_h[0]=PRANDTL(N2,T=T_bar_h[0])
   rho_h[0]=DENSITY(Nitrogen,T=T_bar_h[0],P=P_bar_h[0])
   mu_h[0]=VISCOSITY(Nitrogen,T=T_bar_h[0],P=P_bar_h[0])

"Calculations"
   C_h[0]=m_dot_h*CP_h[0]

"Fin effektiwiteit"
   eta_oh[0]=1-(A_f/A_h)*(1-eta_fh[0])
   eta_fh[0]=(tanh(m_h[0]*(b/2)))/(m_h[0]*(b/2))
   m_h[0]=(2*(h_h[0]/k[0])*((b+t_f)/((b/2)*t_f)))^0.5

"Hitte-oordrags koëffisiente"
   Nu_h[0]=(h_h[0]*D_h)/k_h[0]
   Nu_h[0]=Nu_verkoel(Re_h[0],Pr_h[0])

"Drukval vergelykings"
   V_h[0]=m_dot_h/(rho_h[0]*A_ff)
   Re_h[0]=abs((rho_h[0]*V_h[0]*D_h)/mu_h[0])
   f_h[0]=57/Re_h[0]
   DELTAP_h[0]=(((f_h[0]*L)/D_h+0.5)*((abs(m_dot_h)*m_dot_h)/(2*rho_h[0]*A_ff^2)))
   sigmaK=0
   P_he[0]=P_hi[0]-DELTAP_h[0]
   P_bar_h[0]=(P_hi[0]+P_he[0])/2
   DELTAP_h_t[0]=DELTAP_h[0]
   epsilon_ph=(DELTAP_h_t[j]/P_hi[0])*100

"Globale hitte-oordragskoëffisient"
   1/UA_h[0]=1/(eta_oh[0]*h_h[0]*A_h)
L[0]=L
```

```
duplicate i=1,j-1
"Properties"
   CP_h[i]=CP(Nitrogen,T=T_bar_h[i],P=P_bar_h[i])
   k_h[i]=CONDUCTIVITY(N2,T=T_bar_h[i])
   Pr_h[i]=PRANDTL(N2,T=T_bar_h[i])
   rho_h[i]=DENSITY(Nitrogen,T=T_bar_h[i],P=P_bar_h[i])
   mu_h[i]=VISCOSITY(Nitrogen,T=T_bar_h[i],P=P_bar_h[i])

"Calculations"
   C_h[i]=m_dot_h*CP_h[i]

"Fin effektiwiteit"
   eta_oh[i]=1-(A_f/A_h)*(1-eta_fh[i])
   eta_fh[i]=(tanh(m_h[i]*(b/2)))/(m_h[i]*(b/2))
   m_h[i]=(2*(h_h[i]/k[i])*((b+t_f)/((b/2)*t_f)))^0.5

"Hitte-oordrags koëffisiente"
   Nu_h[i]=(h_h[i]*D_h)/k_h[i]
   Nu_h[i]=Nu_verkoel(Re_h[i],Pr_h[i])

"Drukval vergelykings"
      P_hi[i]=P_he[i-1]
   V_h[i]=m_dot_h/(rho_h[i]*A_ff)
   Re_h[i]=abs((rho_h[i]*V_h[i]*D_h)/mu_h[i])
   f_h[i]=57/Re_h[i]
   DELTAP_h[i]=(((f_h[i]*L)/D_h)*((abs(m_dot_h)*m_dot_h)/(2*rho_h[i]*A_ff^2)))
   P_he[i]=P_hi[i]-DELTAP_h[i]
   P_bar_h[i]=(P_hi[i]+P_he[i])/2
   DELTAP_h_t[i]=DELTAP_h_t[i-1]+DELTAP_h[i]

"Globale hitte-oordragskoëffisient"
   1/UA_h[i]=1/(eta_oh[i]*h_h[i]*A_h)
L[i]=L[i-1]+L
end

"Properties"
   CP_h[j]=CP(Nitrogen,T=T_bar_h[j],P=P_bar_h[j])
   k_h[j]=CONDUCTIVITY(N2,T=T_bar_h[j])
   Pr_h[j]=PRANDTL(N2,T=T_bar_h[j])
   rho_h[j]=DENSITY(Nitrogen,T=T_bar_h[j],P=P_bar_h[j])
   mu_h[j]=VISCOSITY(Nitrogen,T=T_bar_h[j],P=P_bar_h[j])

"Calculations"
   C_h[j]=m_dot_h*CP_h[j]

"Fin effektiwiteit"
   eta_oh[j]=1-(A_f/A_h)*(1-eta_fh[j])
   eta_fh[j]=(tanh(m_h[j]*(b/2)))/(m_h[j]*(b/2))
   m_h[j]=(2*(h_h[j]/k[j])*((b+t_f)/((b/2)*t_f)))^0.5

"Hitte-oordrags koëffisiente"
   Nu_h[j]=(h_h[j]*D_h)/k_h[j]
   Nu_h[j]=Nu_verkoel(Re_h[j],Pr_h[j])
```

```
"Drukval vergelykings"
   P_hi[j]=P_he[j-1]
   V_h[j]=m_dot_h/(rho_h[j]*A_ff)
   Re_h[j]=abs((rho_h[j]*V_h[j]*D_h)/mu_h[j])
   f_h[j]=57/Re_h[j]
   DELTAP_h[j]=(((f_h[j]*L)/D_h+1)*((abs(m_dot_h)*m_dot_h)/(2*rho_h[j]*A_ff^2)))
   P_he[j]=P_hi[j]-DELTAP_h[j]
   P_bar_h[j]=(P_hi[j]+P_he[j])/2
   DELTAP_h_t[j]=DELTAP_h_t[j-1]+DELTAP_h[j]

"Globale hitte-oordragskoëffisient"
   1/UA_h[j]=1/(eta_oh[j]*h_h[j]*A_h)
L[j]=L[j-1]+L


"Cold side"
"Properties"
   CP_c[0]=CP(Nitrogen,T=T_bar_c[0],P=P_bar_c[0])
   k_c[0]=CONDUCTIVITY(N2,T=T_bar_c[0])
   Pr_c[0]=PRANDTL(N2,T=T_bar_c[0])
   rho_c[0]=DENSITY(Nitrogen,T=T_bar_c[0],P=P_bar_c[0])
   mu_c[0]=VISCOSITY(Nitrogen,T=T_bar_c[0],P=P_bar_c[0])

"Calculations"
   C_c[0]=m_dot_c*CP_c[0]

"Fin effektiwiteit"
   eta_oc[0]=1-(A_f/A_h)*(1-eta_fc[0])
   eta_fc[0]=(tanh(m_c[0]*(b/2)))/(m_c[0]*(b/2))
   m_c[0]=(2*(h_c[0]/k[0])*((b+t_f)/((b/2)*t_f)))^0.5

"Hitte-oordrags koëffisiente"
   Nu_c[0]=(h_c[0]*D_h)/k_c[0]
   Nu_c[0]=Nu_verkoel(Re_c[0],Pr_c[0])

"Drukval vergelykings"
   V_c[0]=m_dot_c/(rho_c[0]*A_ff)
   Re_c[0]=abs((rho_c[0]*V_c[0]*D_h)/mu_c[0])
   f_c[0]=57/Re_c[0]
   DELTAP_c[0]=(((f_c[0]*L)/D_h+0.5)*((abs(m_dot_c)*m_dot_c)/(2*rho_c[0]*A_ff^2)))
   P_ci[0]=P_ce[0]-DELTAP_c[0]
   P_bar_c[0]=(P_ci[0]+P_ce[0])/2
   DELTAP_c_t[0]=DELTAP_c[0]
   epsilon_pc=(DELTAP_c_t[j]/P_ce[j])*100

"Globale hitte-oordragskoëffisient"
   1/UA_c[0]=1/(eta_oc[0]*h_c[0]*A_h)

duplicate i=1,j-1
"Properties"
   CP_c[i]=CP(Nitrogen,T=T_bar_c[i],P=P_bar_c[i])
   k_c[i]=CONDUCTIVITY(N2,T=T_bar_c[i])
   Pr_c[i]=PRANDTL(N2,T=T_bar_c[i])
   rho_c[i]=DENSITY(Nitrogen,T=T_bar_c[i],P=P_bar_c[i])
   mu_c[i]=VISCOSITY(Nitrogen,T=T_bar_c[i],P=P_bar_c[i])
```

```
"Calculations"
   C_c[i]=m_dot_h*CP_c[i]

"Fin effektiwiteit"
   eta_oc[i]=1-(A_f/A_h)*(1-eta_fc[i])
   eta_fc[i]=(tanh(m_c[i]*(b/2)))/(m_c[i]*(b/2))
   m_c[i]=(2*(h_c[i]/k[i])*((b+t_f)/((b/2)*t_f)))^0.5

"Hitte-oordrags koëffisiente"
   Nu_c[i]=(h_c[i]*D_h)/k_c[i]
   Nu_c[i]=Nu_verkoel(Re_c[i],Pr_c[i])

"Drukval vergelykings"
   P_ci[i]=P_ce[i-1]
   V_c[i]=m_dot_c/(rho_c[i]*A_ff)
   Re_c[i]=abs((rho_c[i]*V_c[i]*D_h)/mu_c[i])
   f_c[i]=57/Re_c[i]
   DELTAP_c[i]=(((f_c[i]*L)/D_h)*((abs(m_dot_c)*m_dot_c)/(2*rho_c[i]*A_ff^2)))
   P_ci[i]=P_ce[i]-DELTAP_c[i]
   P_bar_c[i]=(P_ci[i]+P_ce[i])/2
   DELTAP_c_t[i]=DELTAP_c_t[i-1]+DELTAP_c[i]

"Globale hitte-oordragskoëffisient"
   1/UA_c[i]=1/(eta_oc[i]*h_c[i]*A_h)
end

"Properties"
   CP_c[j]=CP(Nitrogen,T=T_bar_c[j],P=P_bar_c[j])
   k_c[j]=CONDUCTIVITY(N2,T=T_bar_c[j])
   Pr_c[j]=PRANDTL(N2,T=T_bar_c[j])
   rho_c[j]=DENSITY(Nitrogen,T=T_bar_c[j],P=P_bar_c[j])
   mu_c[j]=VISCOSITY(Nitrogen,T=T_bar_c[j],P=P_bar_c[j])

"Calculations"
   C_c[j]=m_dot_h*CP_c[j]

"Fin effektiwiteit"
   eta_oc[j]=1-(A_f/A_h)*(1-eta_fc[j])
   eta_fc[j]=(tanh(m_c[j]*(b/2)))/(m_c[j]*(b/2))
   m_c[j]=(2*(h_c[j]/k[j])*((b+t_f)/((b/2)*t_f)))^0.5

"Hitte-oordrags koëffisiente"
   Nu_c[j]=(h_c[j]*D_h)/k_c[j]
   Nu_c[j]=Nu_verkoel(Re_c[j],Pr_c[j])

"Drukval vergelykings"
   P_ci[j]=P_ce[j-1]
   V_c[j]=m_dot_c/(rho_c[j]*A_ff)
   Re_c[j]=abs((rho_c[j]*V_c[j]*D_h)/mu_c[j])
   f_c[j]=57/Re_c[j]
   DELTAP_c[j]=(((f_c[j]*L)/D_h+1)*((abs(m_dot_c)*m_dot_c)/(2*rho_c[j]*A_ff^2)))
   P_ci[j]=P_ce[j]-DELTAP_c[j]
   P_bar_c[j]=(P_ci[j]+P_ce[j])/2
   DELTAP_c_t[j]=DELTAP_c_t[j-1]+DELTAP_c[j]
```

```
"Globale hitte-oordragskoëffisient"
   1/UA_c[j]=1/(eta_oc[j]*h_c[j]*A_h)


"Wall"
"Properties"
   k[0]=k(T_wp[0])

"Calculations"
   R_w[0]=(t_w)/(k_w[0]*A_h)
   k_w[0]=k[0]
   T_bar_w[0]=(T_wp[0]+T_wc[0])/2

duplicate i=1,j
"Properties"
   k[i]=k(T_wp[i])

"Calculations"
   R_w[i]=(t_w)/(k_w[i]*A_h)
   k_w[i]=k[i]
   T_bar_w[i]=(T_wp[i]+T_wc[i])/2
end


"Heat transfer and temperatures"
   Q_p[0]=m_dot_h*Cp_h[0]*DELTAT_h[0]
   Q_pw[0]=UA_h[0]*(T_wp[0]-T_bar_h[0])
   Q_w[0]=(1/R_w[0])*(T_wc[0]-T_wp[0])
   Q_cw[0]=UA_c[0]*(T_bar_c[0]-T_wc[0])
   Q_c[0]=m_dot_c*Cp_c[0]*DELTAT_c[0]

   Q[0]=Q_p[0]
   Q[0]=Q_pw[0]
   Q[0]=Q_w[0]
   Q[0]=Q_cw[0]
   Q[0]=Q_c[0]

   DELTAT_h[0]=T_he[0]-T_hi[0]
   T_bar_h[0]=(T_hi[0]+T_he[0])/2
   T_bar_c[0]=(T_ci[0]+T_ce[0])/2
   DELTAT_c[0]=T_ce[0]-T_ci[0]
   Q_total[0]=Q[0]

duplicate i=1,j
   T_he[i-1]=T_hi[i]
   T_ci[i]=T_ce[i-1]

   Q_p[i]=m_dot_h*Cp_h[i]*DELTAT_h[i]
   Q_pw[i]=UA_h[i]*(T_wp[i]-T_bar_h[i])
   Q_w[i]=(1/R_w[i])*(T_wc[i]-T_wp[i])
   Q_cw[i]=UA_c[i]*(T_bar_c[i]-T_wc[i])
   Q_c[i]=m_dot_c*Cp_c[i]*DELTAT_c[i]

   Q[i]=Q_p[i]
   Q[i]=Q_pw[i]
   Q[i]=Q_w[i]
```

```
    Q[i]=Q_cw[i]
    Q[i]=Q_c[i]

    DELTAT_h[i]=T_he[i]-T_hi[i]
    T_bar_h[i]=(T_hi[i]+T_he[i])/2
    T_bar_c[i]=(T_ci[i]+T_ce[i])/2
    DELTAT_c[i]=T_ce[i]-T_ci[i]
    Q_total[i]=Q_total[i-1]+Q[i]
end

"Effektiwiteit"
    C_c=m_dot_c*Cp_c
    C_h=m_dot_h*Cp_h
    Cp_h=CP(Nitrogen,T=T_bar_h,P=P_bar_h)
    Cp_c=CP(Nitrogen,T=T_bar_c,P=P_bar_c)
    T_bar_h=(T_hi[0]+T_he[j])/2
    T_bar_c=(T_ci[0]+T_ce[j])/2
    P_bar_h=(P_hi[0]+P_he[j])/2
    P_bar_c=(P_ci[0]+P_ce[j])/2
    C_min=1204

    epsilon=Q_total[j]/Q_max
    Q_max=C_min*DELTAT_max
        DELTAT_max=T_ce[j]-T_hi[0]
```

B-2 EES RESULTS

Abbreviations

a	-	Cell width
alpha	-	Heat transfer area density
A_f	-	Fin area
A_ff	-	Free-flow area
A_h	-	Heat transfer area of increment
A_h_tot	-	Total heat transfer Area
b	-	Cell height
Cp	-	Specific heat
C	-	Fluid capacity rate
DELTAP	-	Pressure difference
DELTAT	-	Temperature difference
D_h	-	Hydraulic diameter
epsilon	-	Effectiveness
epsilon_p	-	Percentage pressure loss
eta_f	-	Fin effectivity
eta_o	-	Overall fin effectivity
f	-	Fanning friction factor
H	-	Height of recuperator
h	-	Heat transfer coefficient
j	-	Number of increments minus 2
k	-	Thermal conductivity
L	-	Length of increment
L_totaal	-	Length of recuperator
Mass	-	Mass of recuperator
mu	-	Viscosity
m	-	Fin constant
m_dot	-	Flow rate
Nu	-	Nusselt number
n_h	-	Number of unit cells
n_w	-	Number of channels in width
Pr	-	Prandlt number
P	-	Pressure
Q	-	Heat transfer rate
Re	-	Reynolds number
rho	-	Density
R_w	-	Wall resistance
R_f	-	Fouling factor
sigmaK	-	Secondary losses
T	-	Temperature
t_f	-	Fin thickness
t_w	-	Wall thickness
UA	-	Overall heat transfer coefficient
V	-	Velocity
Vol	-	Volume of the recuperator
W	-	Recuperator width

Subscripts

c	-	Cold side
h	-	Hot side
t	-	Total
max	-	Maximum
min	-	Minimum
i	-	Inlet
e	-	Exit
bar	-	Mean
w	-	wall
m	-	material
f	-	Fin
wp	-	Wall at hot side

a=0.001	C_h=1238	L_totaal=0.75	R_fc=0
alpha=714.3	C_min=1165	Mass=2404	R_fh=0
A_f=5.55	DELTAT_max=-432.4	m_dot_c=1.086	sigmaK=0
A_ff=0.074	D_h=0.001	m_dot_h=1.148	T_bar=311.5
A_h=11.1	epsilon=0.9516	n_h=200	T_bar_c=300.3
A_h_tot=222	epsilon_pc=0.2533	n_w=370	T_bar_h=334.4
b=0.001	epsilon_ph=2.884	P_bar_c=803981	t_f=0.0004
Cp_c=1073	H=0.8	P_bar_h=253984	t_w=0.001
Cp_h=1078	j=19	Q_max=-503918	Vol=0.3108
C_c=1165	L=0.0375	rho_m=14180	W=0.518

Element	CP_c	CP_h	C_c	C_h	C_max	C_min	DELTAP_c	DELTAP_c_t	DELTAP_h	DELTAP_h_t	DELTAT_c	DELTAT_h
1	1117	1121	1213	1287	1287	1213	170.2	170.2	588.7	588.7	-16.86	-15.89
2	1113	1117	1277	1283	1283	1277	149.3	319.4	517.4	1106	-17.38	-16.37
3	1109	1113	1273	1278	1278	1273	143.7	463.1	500.8	1607	-17.9	-16.86
4	1104	1109	1268	1274	1274	1268	138	601.2	483.7	2091	-18.41	-17.33
5	1100	1105	1263	1269	1269	1263	132.3	733.5	466.4	2557	-18.91	-17.8
6	1096	1101	1258	1264	1264	1258	126.5	860	448.7	3006	-19.4	-18.26
7	1091	1097	1253	1259	1259	1253	120.6	980.6	430.8	3437	-19.86	-18.7
8	1087	1092	1248	1254	1254	1248	114.8	1095	412.6	3849	-20.31	-19.12
9	1082	1088	1242	1249	1249	1242	108.9	1204	394.2	4243	-20.72	-19.51
10	1078	1083	1238	1244	1244	1238	102.9	1307	375.7	4619	-21.1	-19.86
11	1074	1079	1233	1239	1239	1233	97.03	1404	357.1	4976	-21.44	-20.18
12	1070	1075	1228	1234	1234	1228	91.15	1495	338.5	5315	-21.73	-20.46
13	1066	1071	1224	1229	1229	1224	85.31	1581	319.8	5635	-21.95	-20.68
14	1063	1067	1220	1224	1224	1220	79.55	1660	301.3	5936	-22.12	-20.85
15	1059	1063	1216	1220	1220	1216	73.89	1734	283	6219	-22.21	-20.95
16	1057	1059	1213	1216	1216	1213	68.35	1802	264.9	6484	-22.23	-20.98
17	1055	1056	1211	1213	1213	1211	62.95	1865	247.2	6731	-22.17	-20.94
18	1053	1053	1209	1209	1209	1209	57.73	1923	229.9	6961	-22.02	-20.82
19	1052	1051	1207	1207	1207	1207	52.7	1976	213.1	7174	-21.79	-20.62
20	1051	1049	1207	1204	1287	1213	62.97	2039	257.5	7432	-21.47	-20.35

Element	eta_fc	eta_fh	eta_oc	eta_oh	f_c	f_h	h_c	h_h	k	k_c	k_h	k_w	L
1	0.9995	0.9995	0.9998	0.9998	0.1343	0.1292	159.2	162.6	386.6	0.05342	0.05456	386.6	0.0375
2	0.9995	0.9995	0.9998	0.9998	0.1325	0.1276	156.6	160.2	385.4	0.05256	0.05376	385.4	0.075
3	0.9995	0.9995	0.9998	0.9998	0.1306	0.126	154	157.7	383.9	0.05167	0.05293	383.9	0.1125
4	0.9995	0.9995	0.9998	0.9998	0.1286	0.1242	151.2	155.2	382.2	0.05075	0.05207	382.2	0.15
5	0.9995	0.9995	0.9998	0.9998	0.1266	0.1225	148.4	152.5	380.2	0.04979	0.05117	380.2	0.1875
6	0.9996	0.9995	0.9998	0.9998	0.1245	0.1206	145.4	149.8	377.9	0.0488	0.05025	377.9	0.225
7	0.9996	0.9995	0.9998	0.9998	0.1223	0.1187	142.4	146.9	375.3	0.04777	0.0493	375.3	0.2625
8	0.9996	0.9995	0.9998	0.9998	0.12	0.1167	139.2	144	372.4	0.04671	0.04832	372.4	0.3
9	0.9996	0.9996	0.9998	0.9998	0.1176	0.1146	135.9	141	369.2	0.0456	0.0473	369.2	0.3375
10	0.9996	0.9996	0.9998	0.9998	0.1151	0.1125	132.5	137.8	365.8	0.04447	0.04625	365.8	0.375
11	0.9996	0.9996	0.9998	0.9998	0.1125	0.1102	129	134.6	362	0.04329	0.04517	362	0.4125
12	0.9996	0.9996	0.9998	0.9998	0.1098	0.1079	125.4	131.3	358.1	0.04208	0.04406	358.1	0.45
13	0.9996	0.9996	0.9998	0.9998	0.107	0.1055	121.7	127.9	353.8	0.04084	0.04292	353.8	0.4875
14	0.9996	0.9996	0.9998	0.9998	0.1041	0.1031	117.9	124.4	349.3	0.03955	0.04175	349.3	0.525
15	0.9996	0.9996	0.9998	0.9998	0.1011	0.1005	114	120.8	344.4	0.03824	0.04055	344.4	0.5625
16	0.9996	0.9996	0.9998	0.9998	0.09797	0.09786	110	117.2	339.2	0.0369	0.03933	339.2	0.6
17	0.9996	0.9996	0.9998	0.9998	0.09476	0.09515	105.9	113.5	333.6	0.03553	0.03808	333.6	0.6375
18	0.9996	0.9996	0.9998	0.9998	0.09147	0.09238	101.7	109.7	327.5	0.03414	0.03682	327.5	0.675
19	0.9996	0.9996	0.9998	0.9998	0.0881	0.08954	97.53	105.9	320.6	0.03273	0.03554	320.6	0.7125
20	0.9997	0.9996	0.9998	0.9998	0.08466	0.08665	93.28	102.1	313	0.0313	0.03425	313	0.75

Element	mu_c	mu_h	m_c	m_h	Nu_c	Nu_h	Pr_c	Pr_h	P_bar_c	P_bar_h	P_ce	P_ci	P_he	P_hi
1	0.00003457	0.00003517	75.93	76.73	2.98	2.98	0.7214	0.7225	803046	257406	803131	802961	257111	257700
2	0.0000341	0.00003473	75.43	76.29	2.98	2.98	0.7205	0.7217	803206	256853	803281	803131	256594	257111
3	0.00003362	0.00003428	74.93	75.84	2.98	2.98	0.7194	0.7209	803353	256344	803424	803281	256093	256594
4	0.00003311	0.00003381	74.43	75.39	2.98	2.98	0.7183	0.7199	803493	255851	803562	803424	255609	256093
5	0.00003259	0.00003333	73.92	74.94	2.98	2.98	0.7171	0.7189	803629	255376	803695	803562	255143	255609
6	0.00003205	0.00003282	73.4	74.49	2.98	2.98	0.7157	0.7177	803758	254919	803821	803695	254694	255143
7	0.00003148	0.0000323	72.87	74.03	2.98	2.98	0.7143	0.7164	803882	254479	803942	803821	254263	254694
8	0.00003089	0.00003176	72.34	73.57	2.98	2.98	0.7128	0.7151	803999	254057	804057	803942	253851	254263
9	0.00003027	0.00003119	71.79	73.11	2.98	2.98	0.7113	0.7137	804111	253654	804165	804057	253457	253851
10	0.00002963	0.00003061	71.22	72.63	2.98	2.98	0.7097	0.7122	804217	253269	804268	804165	253081	253457
11	0.00002896	0.00003	70.63	72.15	2.98	2.98	0.7081	0.7106	804317	252902	804365	804268	252724	253081
12	0.00002827	0.00002937	70.02	71.65	2.98	2.98	0.7066	0.7091	804411	252555	804457	804365	252385	252724
13	0.00002755	0.00002872	69.39	71.14	2.98	2.98	0.7052	0.7076	804499	252225	804542	804457	252065	252385
14	0.0000268	0.00002805	68.74	70.62	2.98	2.98	0.7039	0.7062	804582	251915	804621	804542	251764	252065
15	0.00002602	0.00002735	68.06	70.08	2.98	2.98	0.703	0.7049	804658	251623	804695	804621	251481	251764
16	0.00002522	0.00002664	67.36	69.55	2.98	2.98	0.7024	0.7037	804729	251349	804764	804695	251216	251481
17	0.0000244	0.0000259	66.66	69.01	2.98	2.98	0.7022	0.7029	804795	251093	804827	804764	250969	251216
18	0.00002355	0.00002514	65.95	68.49	2.98	2.98	0.7026	0.7023	804855	250854	804884	804827	250739	250969
19	0.00002268	0.00002437	65.26	68	2.98	2.98	0.7035	0.7022	804911	250633	804937	804884	250526	250739
20	0.0000218	0.00002358	64.6	67.57	2.98	2.98	0.7051	0.7025	804969	250397	805000	804937	250268	250526

Element	Q	Q_c	Q_cw	Q_p	Q_pw	Q_total	Q_w	Re_c	Re_h	rho_c	rho_h	R_w	T_bar_c	T_bar_h	T_bar_w
1	-20448	-20448	-20448	-20448	-20448	-20448	-20448	424.5	441.1	3.503	1.093	2.33E-07	496.8	519.8	508.4
2	-21003	-21003	-21003	-21003	-21003	-41451	-21003	430.3	446.7	3.583	1.113	2.34E-07	479.7	503.6	491.8
3	-21548	-21548	-21548	-21548	-21548	-62999	-21548	436.5	452.5	3.669	1.135	2.35E-07	462.1	487	474.7
4	-22078	-22078	-22078	-22078	-22078	-85076	-22078	443.2	458.8	3.763	1.159	2.36E-07	443.9	469.9	457.1
5	-22589	-22589	-22589	-22589	-22589	-107665	-22589	450.3	465.5	3.864	1.185	2.37E-07	425.3	452.3	439
6	-23078	-23078	-23078	-23078	-23078	-130743	-23078	458	472.6	3.973	1.213	2.38E-07	406.1	434.3	420.4
7	-23539	-23539	-23539	-23539	-23539	-154282	-23539	466.2	480.3	4.092	1.243	2.40E-07	386.5	415.8	401.4
8	-23967	-23967	-23967	-23967	-23967	-178249	-23967	475.1	488.5	4.221	1.276	2.42E-07	366.4	396.9	381.9
9	-24357	-24357	-24357	-24357	-24357	-202606	-24357	484.8	497.3	4.362	1.312	2.44E-07	345.9	377.6	362
10	-24704	-24704	-24704	-24704	-24704	-227310	-24704	495.3	506.8	4.515	1.351	2.46E-07	325	357.9	341.8
11	-25000	-25000	-25000	-25000	-25000	-252310	-25000	506.7	517.1	4.682	1.393	2.49E-07	303.7	337.9	321.2
12	-25239	-25239	-25239	-25239	-25239	-277549	-25239	519.1	528.1	4.865	1.439	2.52E-07	282.1	317.6	300.3
13	-25416	-25416	-25416	-25416	-25416	-302965	-25416	532.7	540.1	5.064	1.489	2.55E-07	260.3	297	279.1
14	-25525	-25525	-25525	-25525	-25525	-328490	-25525	547.6	553.1	5.284	1.543	2.58E-07	238.3	276.3	257.8
15	-25560	-25560	-25560	-25560	-25560	-354050	-25560	563.9	567.2	5.524	1.602	2.62E-07	216.1	255.4	236.3
16	-25516	-25516	-25516	-25516	-25516	-379566	-25516	581.8	582.4	5.788	1.667	2.66E-07	193.9	234.4	214.8
17	-25390	-25390	-25390	-25390	-25390	-404956	-25390	601.5	599	6.079	1.737	2.70E-07	171.7	213.4	193.3
18	-25180	-25180	-25180	-25180	-25180	-430136	-25180	623.2	617	6.399	1.813	2.75E-07	149.6	192.6	171.9
19	-24885	-24885	-24885	-24885	-24885	-455022	-24885	647	636.6	6.751	1.896	2.81E-07	127.7	171.8	150.7
20	-24506	-24506	-24506	-24506	-24506	-479528	-24506	673.3	657.8	7.14	1.986	2.88E-07	106	151.3	129.7

Element	T_ce	T_ci	T_he	T_hi	T_wc	T_wp	UA_c	UA_h	V_c	V_h
1	488.4	505.3	511.8	527.7	508.4	508.4	1767	1804	4.19	14.2
2	471	488.4	495.4	511.8	491.8	491.8	1738	1778	4.096	13.94
3	453.1	471	478.6	495.4	474.7	474.7	1709	1750	3.999	13.67
4	434.7	453.1	461.3	478.6	457.1	457.1	1678	1722	3.9	13.39
5	415.8	434.7	443.4	461.3	439	439	1647	1692	3.798	13.09
6	396.4	415.8	425.2	443.4	420.4	420.4	1614	1662	3.693	12.79
7	376.6	396.4	406.5	425.2	401.4	401.4	1580	1630	3.586	12.48
8	356.3	376.6	387.4	406.5	381.9	381.9	1545	1598	3.477	12.16
9	335.5	356.3	367.9	387.4	362	362.1	1508	1564	3.365	11.83
10	314.4	335.5	348	367.9	341.8	341.8	1471	1530	3.251	11.49
11	293	314.4	327.8	348	321.2	321.2	1432	1494	3.135	11.14
12	271.3	293	307.4	327.8	300.3	300.3	1392	1457	3.017	10.78
13	249.3	271.3	286.7	307.4	279.1	279.1	1350	1419	2.898	10.42
14	227.2	249.3	265.8	286.7	257.8	257.8	1308	1381	2.778	10.05
15	205	227.2	244.9	265.8	236.3	236.3	1265	1341	2.657	9.681
16	182.7	205	223.9	244.9	214.8	214.8	1220	1301	2.535	9.307
17	160.6	182.7	203	223.9	193.3	193.3	1175	1259	2.414	8.931
18	138.6	160.6	182.1	203	171.9	171.9	1129	1218	2.294	8.556
19	116.8	138.6	161.5	182.1	150.7	150.7	1082	1175	2.174	8.182
20	95.3	116.8	141.2	161.5	129.7	129.7	1035	1133	2.056	7.812

B-3 FLOWNEX RESULTS

Abbreviations

Cp	-	Specific heat of material
HEAT	-	Heat transfered
M	-	Mach number of fluid
Massource	-	Flow rate
MFlow	-	Flow rate
Mach	-	Mach number of fluid
P	-	Pressure
Rho	-	Density
T	-	Temperature
Vel	-	Velocity of fluid

Subscripts

e	-	Exit
i	-	Inlet
m	-	Mean
p	-	Primary side (Hot side)
s	-	Secondary side (Cold side)

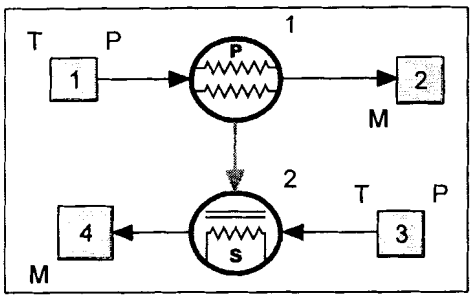

Figure A-1 Flownex Model

NODE NO	P [kPa]	T [°C]	Vel [m/s]	Mach	MASSOURCE [kg/s]
1	257.7	527.7	14.31	0.025	1.148
2	250.44	141.8	7.63	0.018	-1.148
3	805	95.3	1.99	0.005	1.086
4	802.983	505.4	4.22	0.008	-1.086
Effectiveness=0.94843					

Hot Side

ELEM NO	P_i [kPa]	P_e [kPa]	T_i [°C]	T_e [°C]	MFLOW [kg/s]	VEL_i [m/s]	VEL_e [m/s]	VEL_m [m/s]	M_i []	M_e []	AREA_i [m²]	AREA_e [m²]	HEAT [kW]	RHO [kg/m³]	Cp_i [kJ/(kg.K)]	Cp_e [kJ/(kg.K)]
1	257.7	257.17	527.7	511.79	1.15	14.31	14.06	14.19	0.025	0.025	0.074	0.074	-20.299	1.09356	1122.18	1118.33
2	257.17	256.65	511.79	495.49	1.15	14.06	13.79	13.93	0.025	0.025	0.074	0.074	-20.767	1.11398	1118.33	1114.39
3	256.65	256.15	495.49	478.85	1.15	13.79	13.52	13.66	0.025	0.025	0.074	0.074	-21.204	1.13587	1114.39	1110.36
4	256.15	255.67	478.85	461.88	1.15	13.52	13.24	13.38	0.024	0.024	0.074	0.074	-21.622	1.15933	1110.36	1106.35
5	255.67	255.21	461.88	444.46	1.15	13.24	12.95	13.1	0.024	0.024	0.074	0.074	-22.193	1.18459	1106.35	1102.24
6	255.21	254.76	444.46	426.49	1.15	12.95	12.65	12.8	0.024	0.024	0.074	0.074	-22.884	1.212	1102.24	1098
7	254.76	254.33	426.49	407.63	1.15	12.65	12.33	12.49	0.024	0.023	0.074	0.074	-23.528	1.24221	1098	1093.55
8	254.33	253.92	407.63	388.53	1.15	12.33	12	12.17	0.023	0.023	0.074	0.074	-23.819	1.27525	1093.55	1089.04
9	253.92	253.53	388.53	369.22	1.15	12	11.67	11.84	0.023	0.023	0.074	0.074	-24.077	1.31075	1089.04	1084.65
10	253.53	253.15	369.22	349.6	1.15	11.67	11.33	11.5	0.023	0.022	0.074	0.074	-24.46	1.34905	1084.65	1080.43
11	253.15	252.8	349.6	329.62	1.15	11.33	10.98	11.16	0.022	0.022	0.074	0.074	-24.921	1.39065	1080.43	1076.13
12	252.8	252.47	329.62	308.97	1.15	10.98	10.62	10.8	0.022	0.022	0.074	0.074	-25.316	1.43632	1076.13	1071.69
13	252.47	252.15	308.97	288.19	1.15	10.62	10.25	10.44	0.022	0.021	0.074	0.074	-25.401	1.48653	1071.69	1067.23
14	252.15	251.85	288.19	267.4	1.15	10.25	9.88	10.07	0.021	0.021	0.074	0.074	-25.409	1.54075	1067.23	1063.35
15	251.85	251.57	267.4	246.49	1.15	9.88	9.51	9.7	0.021	0.021	0.074	0.074	-25.561	1.59952	1063.35	1060.15
16	251.57	251.31	246.49	225.5	1.15	9.51	9.14	9.33	0.021	0.02	0.074	0.074	-25.641	1.66354	1060.15	1056.94
17	251.31	251.07	225.5	204.23	1.15	9.14	8.76	8.95	0.02	0.02	0.074	0.074	-25.62	1.73387	1056.94	1053.68
18	251.07	250.84	204.23	183.18	1.15	8.76	8.38	8.57	0.02	0.019	0.074	0.074	-25.357	1.81077	1053.68	1050.46
19	250.84	250.63	183.18	162.36	1.15	8.38	8	8.19	0.019	0.019	0.074	0.074	-25.09	1.89416	1050.46	1048.31
20	250.63	250.44	162.36	141.79	1.15	8	7.63	7.82	0.019	0.018	0.074	0.074	-24.777	1.98477	1048.31	1046.62

Cold Side

ELEM NO	P_i [kPa]	P_e [kPa]	T_i [°C]	T_e [°C]	MFLOW [kg/s]	VEL_i [m/s]	VEL_e [m/s]	VEL_m [m/s]	M_i []	M_e []	AREA_i [m²]	AREA_e [m²]	HEAT [kW]	RHO [kg/m³]	Cp_i [kJ/(kg.K)]	Cp_e [kJ/(kg.K)]
1	805	804.95	95.3	117.21	1.09	1.99	2.11	2.05	0.005	0.005	0.074	0.074	24.777	7.14842	1042.81	1044.61
2	804.95	804.9	117.21	139.3	1.09	2.11	2.23	2.17	0.005	0.005	0.074	0.074	25.09	6.75558	1044.61	1046.42
3	804.9	804.84	139.3	161.55	1.09	2.23	2.35	2.29	0.005	0.006	0.074	0.074	25.357	6.40217	1046.42	1048.24
4	804.84	804.78	161.55	184.03	1.09	2.35	2.47	2.41	0.006	0.006	0.074	0.074	25.62	6.08064	1048.24	1050.6
5	804.78	804.71	184.03	206.52	1.09	2.47	2.6	2.54	0.006	0.006	0.074	0.074	25.641	5.78825	1050.6	1054.04
6	804.71	804.63	206.52	228.92	1.09	2.6	2.72	2.66	0.006	0.006	0.074	0.074	25.561	5.5229	1054.04	1057.47
7	804.63	804.55	228.92	250.89	1.09	2.72	2.84	2.78	0.006	0.006	0.074	0.074	25.409	5.28374	1057.47	1060.83
8	804.55	804.47	250.89	272.86	1.09	2.84	2.96	2.9	0.006	0.006	0.074	0.074	25.401	5.06625	1060.83	1064.19
9	804.47	804.38	272.86	294.75	1.09	2.96	3.08	3.02	0.006	0.006	0.074	0.074	25.316	4.86623	1064.19	1068.65
10	804.38	804.28	294.75	316.3	1.09	3.08	3.19	3.13	0.006	0.006	0.074	0.074	24.921	4.68301	1068.65	1073.28
11	804.28	804.18	316.3	337.24	1.09	3.19	3.31	3.25	0.006	0.007	0.074	0.074	24.46	4.51581	1073.28	1077.78
12	804.18	804.07	337.24	357.65	1.09	3.31	3.42	3.36	0.007	0.007	0.074	0.074	24.077	4.36554	1077.78	1082.17
13	804.07	803.95	357.65	377.84	1.09	3.42	3.53	3.47	0.007	0.007	0.074	0.074	23.819	4.22667	1082.17	1086.53
14	803.95	803.83	377.84	397.79	1.09	3.53	3.64	3.58	0.007	0.007	0.074	0.074	23.528	4.09774	1086.53	1091.24
15	803.83	803.7	397.79	417.18	1.09	3.64	3.74	3.69	0.007	0.007	0.074	0.074	22.884	3.9787	1091.24	1095.82
16	803.7	803.57	417.18	435.8	1.09	3.74	3.84	3.79	0.007	0.007	0.074	0.074	22.193	3.86944	1095.82	1100.21
17	803.57	803.43	435.8	453.74	1.09	3.84	3.94	3.89	0.007	0.007	0.074	0.074	21.622	3.77081	1100.21	1104.44
18	803.43	803.29	453.74	471.33	1.09	3.94	4.04	3.99	0.007	0.007	0.074	0.074	21.204	3.6791	1104.44	1108.6
19	803.29	803.14	471.33	488.56	1.09	4.04	4.13	4.08	0.007	0.007	0.074	0.074	20.767	3.59339	1108.6	1112.73
20	803.14	802.98	488.56	505.4	1.09	4.13	4.22	4.18	0.007	0.008	0.074	0.074	20.299	3.51324	1112.73	1116.81